Characterizing Sierra Nevada Snowpack Using Variable-Resolution CESM

Alan M. Rhoades*, Xingying Huang, and Paul A. Ullrich

University of California, Davis, Davis, California

Colin M. Zarzycki

National Center for Atmospheric Research, Boulder, Colorado

**Corresponding author address:* Alan M. Rhoades, University of California, Davis, Department of Land, Air, and Water Resources (LAWR), Davis, CA 95616

E-mail: amrhoades@ucdavis.edu

ABSTRACT

The location, timing, and intermittency of precipitation in California makes the state integrally reliant on winter season snowpack accumulation to maintain its economic and agricultural livelihood. Of particular concern, winter season snowpack has shown a net decline across the western USA over the past 50 years resulting in a major uncertainty in water resource management heading into the next century. Cutting edge tools are available to help navigate and preemptively plan for these uncertainties. This paper uses a next-generation modeling technique, variable-resolution global climate modeling within the Community Earth System Model (VR-CESM), at horizontal resolutions of 0.125° (14km) and 0.25° (28km). VR-CESM provides means to include dynamically large-scale atmosphere-ocean drivers, limit model bias, provide more accurate representations of regional topography, while doing so in a more computationally efficient manner than conventional general circulation models. This paper validates VR-CESM at climatological and seasonal timescales for Sierra Nevada snowpack metrics by comparing them to the DAYMET, CAL-ADAPT, NARR, NCEP, and NLDAS reanalysis datasets, the MODIS remote sensing dataset, SNOTEL observational dataset, a standard practice global climate model (CESM) and regional climate model (WRF) dataset. Overall, considering California's complex terrain, intermittent precipitation, and that both of the VR-CESM simulations were only constrained by prescribed sea surface temperatures and sea ice extent data, a 0.68 centered Pearson product-moment correlation, negative mean SWE bias of <7 mm, interquartile range well within the values exhibited in the reanalysis datasets, and mean DJF SNOWC within 7% of the expected MODIS value, the efficacy of the VR-CESM framework is apparent.

1. Introduction

California receives half of its total annual precipitation in five to fifteen days of the year, making its precipitation patterns some of the most intermittent in the USA (Dettinger et al. 2011). Importantly, most of the state's precipitation falls during the winter months (December to February) and two-thirds of it precipitates in the northern and mountainous parts of the state (Wise 2012). The precipitation that falls in the mountainous region largely accumulates as snow (Pandey et al. 1999). Thus, winter snowpack acts as a natural surface reservoir for water that is then released during dry portions of the year. Snowpack provides approximately three-fourths of the annual fresh water supply in the western USA (Palmer 1988; Cayan 1996), and 60% of California's developed water supply originates from the snowpack dominated Sierra Nevada (Bales et al. 2011). Along with the Colorado River, this natural store of water contributes to the maintenance of California's economy and its stance as one of the largest agricultural providers in the world (Tanaka et al. 2006; Hanak and Lund 2012). These water reserves also provide up to 21% of the energy found within California's diverse energy portfolio via hydroelectric plants (Stewart 1996). Therefore, the integrity of California's economy, and agricultural identity, is largely dependent on ample snowpack accumulation in the Sierra Nevada.

A major cause of interannual variability in winter precipitation in California, and the greater western USA, are global teleconnections. Teleconnections are recurrent and persistent atmosphere-ocean patterns impacting large swaths of latitudinal and longitudinal bands (Wallace and Gutzler 1981; Glantz et al. 1991). They are important from a water resources perspective because they determine overall temperature, precipitation, and snowpack trends within California. Atmosphere-ocean climate interactions have been found to vary annual precipitation by 20-45% in the western USA (Dettinger et al. 1998), and include the El Niño Southern Oscillation (ENSO), the

Pacific Decadal Oscillation (PDO), the Pacific North American Pattern (PNA), the North American Monsoon, and the Aleutian Low, as well as more short term events known as atmospheric rivers (ARs) (i.e., equatorially generated whip-like water vapor bands) (Dettinger et al. 1998; Cayan et al. 1999; Ralph et al. 2004; Dettinger 2011; Wise 2012; Guan et al. 2013; Fang et al. 2014). The internal variability associated with teleconnections modulate the spatial and temporal variability of strong precipitation events in the western USA (Wise 2012). Therefore, teleconnection modulation, on both yearly and decadal time frames, has a direct impact on the amount of total seasonal snowpack deposited in the Sierra Nevada. This modulation is also essential in resolving historical trends as well as projecting future snowpack tendencies. For example, atmospheric rivers alone account for around 30-40% of seasonal snowpack accumulation in the Sierra Nevada (Guan et al. 2010). Thus, a representation of global processes, ideally via a global climate model, is necessary to accurately account for California's temperature, precipitation, and snowpack trends.

To observe how this crucial natural fresh water reserve is characterized, both spatially and temporally, snowpack metrics such as snow water equivalent (SWE), snow centroid date (SCD), and the extent of snow cover (SNOWC) have been developed to quantify the patterns of Sierra Nevada snowpack. SWE is used to determine the total water content for a given snow depth. It can be quantified by taking a given depth of snow and melting it; the resultant water content represents the SWE. This is useful since snow densities can fluctuate due to variations in snowfall as well as melt and ablation events in the snowpack. SCD represents the date of peak snowpack accumulation, which is useful in understanding snowmelt onset. SNOWC characterizes the total areal coverage of snow over a given region. This is helpful in quantifying shifts in regional to global albedo as well as the freezing line extent in mountainous environments. Over the historical record, the Sierra Nevada has shown a mean difference in April 1st SWE of 2.2% (i.e., northern Sierra decline of 50-75% and southern Sierra accumulation of 30%) (Mote et al. 2005), western USA

SCD was found to shift 0.7 days earlier per decade (Kapnick and Hall 2012), and total SNOWC declined by 9% across the Northern Hemisphere (Rupp et al. 2013). The shift in SCD appears to be eight days earlier per °C of warming in end of winter season (March and April) temperatures. Additionally, Bales et al. (2006) found that the fraction of storms that occur with surface temperatures in the range of -3 °C to 0 °C account for up to 36% of the annual precipitation events in many parts of the Sierra Nevada, highlighting the sensitivity of snow storms in the Sierra Nevada to increasing temperatures due to anthropogenic global climate change. Using IPCC AR5 RCP 4.5 and 8.5 scenarios, projected end-of-the-century trends for snowpack highlight that western USA SWE may decline by 40-70% (Pierce and Cayan 2013), snowfall may decrease by 25-40% (Pierce and Cayan 2013), more winter storms may tend towards rain rather than snow (Bales et al. 2006), and relatively warmer storms (e.g., atmospheric rivers) may be more frequent and intense for California (Dettinger 2011). In a review paper by Gimeno et al. (2014), Dettinger et al. (2011) represented the only western USA specific paper on the future projected trends of ARs. Of note, the authors expressed that the results in this study were a preliminary step and should be assessed more from a qualitative sense due to the small sample size of AR events in the CMIP5 archive and the various assumptions associated with the relatively coarser temporal and spatial extents of the models in the CMIP5 archive. Therefore, if the aforementioned projected outcomes hold, mean precipitation is not expected to change dramatically, but interannual variability will likely increase through modulation in atmospheric river events. Since snowpack is affected by both precipitation and temperature, it is expected that increased end-of-century temperatures coupled with more intense warmer storms in the western USA will prevent snow accumulation and lead to changes in runoff timing that could be problematic for water management. Thus, an analysis of causal mechanisms of snowpack accumulation and snowmelt timing, with a dynamic inclusion of large-scale atmosphere-ocean drivers, and an accurate representation of the complex topography of California is needed to allow water managers to make more informative and preemptive decisions on Californias water future.

One key approach to address the aforementioned need is via climate models. However, both global and regional climate models have limitations in their predictive capacities. As demonstrated by the North American Regional Climate Change Assessment Program (NARCCAP), regional climate models (RCMs) were shown to produce too dry, too warm, and too little SWE conditions for the western USA and snow cover duration was found to start too late and end too early (Salzmann and Mearns 2012). Model bias was associated with inadequate topography representation, imperfections in observational data, and differing land surface model components (Salzmann and Mearns 2012). Similarly, Caldwell (2010) found that RCMs generally overpredict winter precipitation in California, whereas global climate models (GCMs) generally underpredict winter precipitation in California. The precipitation bias associated with GCMs was not solely related to model resolution (as this was standardized before comparison), but rather factors such as subgrid-scale parameterizations and coarse model topography too (Caldwell 2010). The aforementioned RCM findings regarding precipitation and SWE appear contradictory to one another, but it should be noted that California hydroclimatic trends have shown dissimilarities from several of those shown in other parts of the western USA (Mote et al. 2005; Kapnick and Hall 2012), likely due to a combination of relatively higher topographical elevation in the southern Sierra Nevada (compared to other western USA mountain ranges), proximity to the Pacific Ocean, and effects from ARs.

This paper aims to analyze the efficacy of variable-resolution modeling using the Community Earth System Model (VR-CESM) at resolutions of 0.125° (14km) and 0.25° (28km) in representing Sierra Nevada snowpack, in comparison with observational, reanalysis and dynamically downscaled model results. Variable-resolution modeling is a novel tool for modeling the climate system and represents a hybrid of global and regional climate models. We envision that this new modeling framework will bring added value to the snowpack modeling community with the benefit of a global solution, accounting for major teleconnections, and regional high-resolution, better representation of winter storms and orographic forcings. This hypothesis has been corroborated for temperature and precipitation climatic trends within California in Huang et al. (2015). These benefits will lead to a better representation of observed summary statistics for winter snowpack within a GCM framework. Further, several studies have shown that CESM has skill in representing the major wintertime teleconnections of the western USA including the ENSO (DeFlorio et al. 2013; Wang et al. 2014), the PDO (DeFlorio et al. 2013), and the Pacific-North American (PNA) pattern (Li and Forest 2014). Teleconnection representation in these studies is expected to carry over into VR-CESM.

The structure of the remainder of the paper is as follows: Section 2 contains information about the CESM setup and experimental design, including VR-CESM grid implementation. Section 3 discusses the comparative datasets used to assess model efficacy. Section 4 provides summary statistic comparisons of seasonal to multidecadal snow trends, including SWE and SNOWC. Finally, section 5 provides further discussion and the conclusions of this study.

2. CESM Setup and VR-CESM Grid Implementation

CESM Setup

This project utilized version 1.2 of the Community Earth System Model (CESM), a widely used and community-supported climate model developed by the National Center for Atmospheric Research (NCAR) and the US Department of Energy (DoE). CESM is a fully coupled global climate model comprised of seven geophysical models that simulate the major components of the Earth system including the atmosphere, land-surface, land-ice, ocean, ocean-wave, river run-off and sea ice, all of which can be coupled dynamically. One of the F-component sets in CESM, FAMIPC5, is the standard protocol for the Atmospheric Model Intercomparison Project (AMIP) and was used for each of the CESM simulations in this study (Gates 1992). This component set consists solely of the atmosphere-land coupled model with prescribed sea-surface temperatures (SSTs) and sea ice extent. This limited configuration maximizes computational efficiency and inhibits model bias propagation. This is advantageous for a local server environment ($<$1000 processors per simulation), like the one used in this study. Although the oceanic and sea ice systems were not incorporated dynamically into this study, this component set ensures that interannual climate variability (mainly via SST anomalies) and global albedo effects from sea ice extent are incorporated into the simulations. Future research will target the VR-CESM simulation performance with and without a dynamic ocean model. Thus, for this study, only the atmosphere model (Community Atmosphere Model (CAM) version 5.3) (Neale et al. 2010) and the land-surface model (Community Land Model (CLM) version 4.0 with satellite phenology) (Oleson et al. 2010) were utilized.

CAM was run with the Spectral Element (SE) dynamical core with a cubed-sphere grid structure (Taylor et al. 1997; Dennis et al. 2011). CAM-SE uses a continuous Galerkin spectral finite-element method for solving the hydrostatic atmospheric primitive equations. CAM-SE provides several benefits over other CESM dynamical cores including linear scalability with increasing computer processor counts, machine precision conservation of mass and tracers, elimination of non-uniform grid spacings due to convergence zones at higher latitudes, and variable-resolution capabilities (Taylor and Fournier 2010; Dennis et al. 2011; Zarzycki et al. 2014a,b; Zarzycki and Jablonowski 2014). CAM5 physics are broken down into six main categories: shallow convection (Park and Bretherton 2009), deep convection (Neale et al. 2008), microphysics (Morrison and Gettelman 2008), macrophysics (Park et al. 2014), radiation (Iacono et al. 2008), and aerosols (Ghan et al. 2012). Details on each of the physics schemes can be found in Neale et al. (2010).

CLM subdivides each cell into land types such as glacier, lake, urban, vegetated, and wetland (Oleson et al. 2010; Lawrence et al. 2011). The vegetated component of the grid cell is further broken down into various soil types which are then characterized by 16 unique Plant Functional Types (PFTs), including non-vegetated. CLM4.0 PFTs include five evergreen species and six deciduous species for temperate, boreal, and tropical climates, three grasses for arctic and non-arctic climates (with C-3 and C-4 variations) and a few staple cereal crops. PFT cover is derived from the Moderate Resolution Imaging Spectroradiometer (MODIS) satellite data at 0.5° resolution with canopy heights for each of the PFTs assumed to range from 0.5 meters (crops, grasses, and shrubs) to 35 meters (trees). PFT types and percent cover of PFTs within each vegetated land-unit play a crucial role in shaping snowpack trends. This is because the interaction between the canopy and snowpack are PFT specific for biogeochemical, radiative, and hydrological processes such as interception, throughfall, canopy drip, water removal via transpiration, and optical property interactions based on leaf angle and specific PFT (Lawrence et al. 2011).

The parameterizations of snowpack within CESM are based primarily on work done by Anderson (1976), Jordan (1991), and Yongjiu and Qingcun (1997). These parameterizations characterize several important state variables for snowpack including the mass of water, mass of ice, snowpack layer thickness, temperature profile of the snowpack layer, black carbon and mineral deposition, and snowpack aging and optical properties. The model is discretized using five snow layers with dynamic compaction, water transfer, and energy transfer.

VR-CESM Grid Implementation

The VR-CESM grids were generated using a freely available software package (SQuadGen) (Ullrich 2014). To generate the variable-resolution grid files, SQuadGen interpolates a picture image file, with variations in its gray scale properties, creates a refinement map, and uses spring dynamics to smooth the transitional regions between various grid resolutions. VR-CESM 0.25° (28km resolution) and VR-CESM 0.125° (14km resolution) grids were constructed for both CAM and CLM (Figure 1). Topographic smoothing was varied between the two VR-CESM 0.25° simulations (VR-CESM 0.25° (smooth) and VR-CESM 0.25° (rough)) without modifying the grid structure to assess the sensitivity of topographical influences on VR-CESM simulations. This study further represents the first time variable-resolution grids were implemented into CLM.

Topographic Representation in the VR-CESM Simulations

Topographical datasets were generated for each variable resolution grid. The topographic smoothing was varied between the two VR-CESM 0.25° simulations by adjusting the c parameter from Eqn. (1) in Zarzycki et al. (2015). In the case of the VR-CESM 0.25° (smooth) topography, this parameter was equal to 1.33 times that used for generating VR-CESM 0.25° (rough) case. This resulted in the differences in topographical representation seen in Figs. 2a-b. Careful consideration is required when generating the VR-CESM topographical datasets due to the fact that CAM-SE uses terrain-following vertical coordinates that exhibit, with excessive terrain roughness, a tendency towards generation of spurious vertical velocities and numerical artifacts (Zarzycki et al. 2015). The topographical datasets were derived using bilinear interpolation with a linear smoothing operator on the 2-minute National Geophysical Data Center (NGDC) Gridded Global Relief Dataset (ETOPO2v2) (National Geophysical Data Center 2006) coinciding with the variable-resolution grids surface geopotential and order of the hyperviscosity term. This provides more (less) topographical structure in the high (low) resolution region of the nest. For example, maximum Sierra Nevada topographical elevations (see Figure 2) in the 111 km, 28 km, and 14 km resolutions of CESM were 1583.31 meters, 2677.08 meters, and 3147.28 meters, respectively.

When compared with the ETOPO2v2 NGDC dataset, topographical elevation in the Sierra Nevada matches more closely as model resolution increases (Figure 2).

3. Reference Datasets and Statistical Methods

Reference Datasets

Observational datasets for snowpack metrics such as snow water equivalent (SWE) and snow cover (SNOWC) are particularly difficult to develop in mountainous environments. The fractal nature of snowpack deposits, quick shifts in elevation, angular differences in topography, alpine vegetation cover, cloud cover, and large footprint radius associated with satellite instrumentation are key challenges. Additionally, many satellite products span less than a decade, preventing analysis of climate patterns over decadal timeframes. In situ measurements help alleviate some of the highlighted issues, yet they are irregularly located, and so may not be representative in regions of rapidly varying topography. Land surface models have been used to abate the discontinuous nature of in situ observations, but often contain their own biases. Therefore, to provide a rigorous assessment, a blend of the aforementioned data types will be used in this assessment.

The datasets that this study used for validation purposes are listed in Table 1. Datasets vary in snowpack product availability (i.e., SWE and SNOWC), spatial and temporal resolution, map projection, and temporal range. Therefore, all datasets were standardized to monthly averaged, seasonally averaged (DJF), and climate averaged (DJF from 1980-2005) temporal resolutions during the assessment of the VR-CESM simulations. In order to accomplish this task, utilities from the NetCDF Operators (NCO), Climate Data Operators (CDO), and the NCAR Command Language (NCL) were used.

The North America Land Data Assimilation System Phase 2 (NLDAS-2) produced 0.125° datasets by incorporating large quantities of observational and model reanalysis datasets into three non-atmosphere coupled land-surface models (i.e., Princeton's implementation of VIC, NOAA's Noah, and NASA's Mosaic) over the continental United States. The three datasets provide SWE and SNOWC and are extensively analyzed by Xia et al. (2012a,b). For the 2008 California climate change assessment, four GCM (i.e., CCSM3, CNRM, GFDL, and PCM1) datasets were downscaled using Bias Corrected Statistical Downscaling (BCSD) methods along with the VIC model at a resolution of 0.125°. This dataset, known as CAL-ADAPT, provides SWE values over the entirety of California, with the methodology discussed in Maurer and Hidalgo (2008). The DAYMET dataset provides SWE estimations based on meteorological stations. The station data is then extrapolated, using a truncated Guassian weighting filter, to create a high resolution gridded output (Thornton et al. 2014). The Moderate Resolution Imaging Spectroradiometer (MODIS) satellite remote sensing dataset (MODIS/Terra Snow Cover Monthly 0.05° (5 km), Version 5 (MOD10CM V005)) provides SNOWC using a snow mapping algorithm with a Normalized Difference Snow Index (NDSI) (Hall et al. 2006). The NDSI is used to distinguish between snow and other features (such as cloud cover) by using visible and short-wave near-IR spectral bands. A comprehensive analysis and validation of the MODIS dataset for a region of the Sierra Nevada was conducted in Hall and Riggs (2007). The SNOwpack TELemetry (SNOTEL) in situ dataset is comprised of 32 automated observational stations spread throughout the Sierra Nevada mountain range measuring SWE (Serreze et al. 1999). The areal extent of the SNOTEL stations range from 38.07° to 42.99° latitude by -120.79° to -119.23° with an average elevation of 2,343 meters. Of the 32 stations, only 19 were utilized as they spanned the entire 1980-2005 temporal range. The North American Regional Reanalysis (NARR) dataset provides monthly averaged SNOWC output variables using a high resolution atmospheric model (Eta Model) forced by a Regional Data Assimilation System

(RDAS) (Mesinger et al. 2006). The other reanalysis dataset used (NCEP - CFSV2) is an updated version (2013) of its predecessor (2004) and provided SNOWC data (Saha et al. 2014). The NCEP dataset provides better representations of 2m surface temperature, Madden-Julian Oscillation (MJO), and SST forecasts while upgrading overall performance in seasonal to subseasonal forecasting results, compared to its predecessor, and has been advised for decision makers in the water management and agricultural sectors (Saha et al. 2014).

A 0.25° (finite volume) and 1° (spectral element) uniform resolution CESM run were used for comparison to the VR-CESM simulations as well. The 0.25° simulation is described in Wehner et al. (2014) and the 1° simulation was performed by the research team with the same component set and dynamical core as the VR-CESM simulations. The final datasets utilized for this assessment were a pair of simulations conducted at UC Davis using the Weather Research and Forecast (WRF) model, which has been used extensively for regional climate studies. Several common parameterization combinations (including different cumulus schemes and radiation schemes) were tested over a one-year simulation period and compared with gridded observations. Those final options were chosen for climate applications that balance long-term reliability and computational cost, representing a typical RCM configuration. Subgrid parameterizations include: the Kain-Fritsch cumulus scheme (Kain 2004), the WSM 6-class graupel microphysics scheme (Hong and Lim 2006), and the CAM short-wave and long-wave radiation schemes (Collins et al. 2004). The simulations used a nested domain with a coarse resolution of 27km (WRF-27) and a finer resolution domain of 9km (WRF-9) situated over the western USA (centered over the Sierra Nevada). The initial, boundary conditions, and sea surface temperatures were all provided by ERA-Interim reanalysis data, a widely used and validated dataset for this type of work (Dee et al. 2011). Both WRF domains provide SWE and SNOWC output variables via the Noah Land Surface Model

(Chen and Dudhia 2001) coupled with the Yonsei University (YSU) boundary layer scheme (Hong et al. 2006).

The Noah and CLM4.0-SP land surface models (LSMs) derive from similar snow model formulations (i.e., Anderson (1976)), yet deviate in several ways too. The Noah LSM pulls primarily from Yen (1965), whereas CLM4.0-SP draws from Jordan (1991). This creates differences in both of the snow model's fundamental equations and parameterizations. Differences include number of snow layers (Noah LSM has three, whereas CLM4.0-SP has five), snow thermal conductivity (CLM4.0-SP uses a snow density function and Noah LSM uses a constant), snow cover hyperbolic functions (CLM4.0-SP utilizes a slightly more complicated formulation) and snowpack-canopy interactions (Oleson et al. 2010; Yang et al. 2011). Of relevance to this paper's overall conclusions, snow depths (and thus SWE) estimations in the Noah LSM have been noted to be significantly overestimated in certain cases due to the assumption that snowpack density, physical characteristics, and thermal conductivity are constant, therefore neglecting heat transfers via meltwater movement in the snowpack (Yang et al. 2011).

Statistical Methods

The DJF climatological mean state and seasonal variability in snow products found within the Sierra Nevada were analyzed. The assessment aimed to understand the efficacy of the new VR-CESM approach in representing snowpack trends against observation, reanalysis and other widely used GCMs and RCMs. In order to do this, the datasets were remapped to similar map projections and resolutions using both the Earth System Modeling Framework (ESMF) capabilities in the NCAR Command Language (NCL) and TempestRemap (Ullrich and Taylor 2015) software suites. The observational and reanalysis datasets were further remapped to all possible resolutions used in the models (i.e., 0.125°, 0.25°, and 1°). The climate averages and seasonal averages were computed using a mask of the Sierra Nevada (see Figure 3). This mask was developed by the EPA's Ecoregions classification system (Ecoregion Level III - 6.2.12). Summary statistics of the Sierra Nevada were calculated for each of the datasets for SWE and SNOWC including mean, standard deviation, lower quartile, median, upper quartile, and maximum.

For most of the datasets assessed, 25 seasons of average DJF values were used. WRF-9 had 22 DJF seasons. Additionally, MODIS had 12 DJF seasons, many of which fall outside the historical period (1980-2005 vs 2000-2012), but due to the scope of this paper in analyzing the climatological and seasonal mean trends (rather than precise seasonal forecasting) this was assumed to be largely irrelevant.

4. Seasonal and Multidecadal Snow Trends in the Sierra Nevada

Snow Water Equivalent Summary Statistics

A panel plot of the DJF average SWE is shown across datasets for California (Figure 4). Clear resolution dependence is apparent across all modeling platforms. Each of the datasets highlighted an overall increasing trend in SWE with an increase in model resolution, likely correlated with topographical representation (see Figure 2) and resultant orographic forcing on weather fronts as well as sustained below-freezing temperatures. Of note, the NCEP dataset didn't characterize enough SWE for the Sierra Nevada region to be further assessed in greater statistical detail. Each of the model datasets are compared to the average of the reanalysis datasets at their closest respective resolution of 0.125°, 0.25°, or 1°. Within the Sierra Nevada masked region, VR-CESM 0.125° and VR-CESM 0.25° (rough) demonstrated the closest statistical match across all observational and reanalysis datasets with mean DJF SWE absolute bias values of 6.4 and 2.7 mm, respectively (the reanalysis dataset average SWE value was 97.4 mm), and median values within 8 to 13 mm (Table

2). Maximum DJF SWE values were most closely represented by CESM-FV 0.25° and VR-CESM 0.25° (rough), both within 68 mm. It should be noted that an artificial cap on maximum SWE at 1,000 mm is imposed in CLM4.0 which impacted maximum SWE values for all VR-CESM and UNIFORM CESM simulations. CESM-FV 0.25° and WRF-9 both showed a positive bias in DJF SWE values for mean and median compared to the reanalysis dataset average. CESM-FV 0.25° had a positive bias of 1.8 times the mean DJF SWE and 2.4 times the median value for the Sierra Nevada mask. WRF-9 exhibited a similar response with a positive bias of 2.4 times the mean and 1.4 times the median DJF SWE. The coarser resolution version of VR-CESM and WRF had a negative bias with VR-CESM 0.25° (smooth) at half the mean for DJF SWE in the Sierra Nevada and WRF-27 at 74%. CESM-SE 1°, the model resolution used in most IPCC simulations, was unable to represent both climatological and seasonal DJF SWE trends in the Sierra Nevada with a maximum DJF SWE value of 41.7 mm (<5% of the reanalysis dataset average maximum value), with similar tendencies seen in the mean and median values as well.

Seasonal Variability in Snow Water Equivalent

SWE DJF mean seasonal variability is represented via a plot of standard deviation at each grid point across all datasets (Figure 5). Characterization of interseasonal variability, in comparison to the reanalysis datasets, was shown to be more difficult for most of the modeling platforms. VR-CESM simulations were best represented by VR-CESM 0.25° (rough) which exhibited a slight positive bias of 1% to the reanalysis dataset average (Table 2). VR-CESM 0.125° and VR-CESM 0.25° (smooth) were at 87% and 36% of the standard deviation, respectively. CESM-FV 0.25° had a large discepency in standard deviation tendency with a positive bias of two times the reanalysis dataset average of the reanalysis datasets. WRF-9 showed an exceedingly high variability with 6.8 times the standard deviation of the reanalysis dataset average, although this could be partially amplified by the fact that DAYMET and CESM SWE values were capped at 1,000 mm. Although the standard deviation values were highly variable across modeling platforms in comparison to the reanalysis dataset average, the average seasonal interquartile ranges (IQR) were more closely aligned (Figure 6). The IQR for VR-CESM 0.125° and VR-CESM 0.25° (rough) were closest to the reanalysis dataset average with a slightly negative bias of 11 mm and 7.8 mm, respectively. WRF-9 and CESM-FV 0.25° had a positive bias in IQR, with exceedingly high 75th percentiles, whereas VR-CESM 0.25° (smooth) and WRF-27 were conservative in their higher quartile marks.

Pattern Correlation and Bias in Snow Water Equivalent

The average DJF centered Pearson product-moment coefficients, or the average statistical similarity between two datasets at identical locations for SWE across the 25 seasons (with removal of the mean), for all of the simulations were computed against each of the remapped reference datasets for the Sierra Nevada masked region (Table 3). The Pearson product-moment coefficients are calculated by computing the covariance of the two datasets and dividing by the product of their standard deviations. Averaging all of the Pearson product-moment coefficients across all grid-points within the mask is useful in showing the seasonal similarity in SWE trend across the entire Sierra Nevada. Interestingly, the VR-CESM simulations were almost identical in average seasonal correlation compared to the reanalysis datasets (at around 0.67 to 0.71) for the Sierra Nevada. WRF-9, remapped to 0.125° (14km) resolution, showed the highest seasonal correlation at 0.83. However, this was not unexpected considering the WRF simulations were forced by ERA-interim data. Both CESM-FV 0.25° and CESM-SE 1° had the lowest correlation with 0.28 and 0.19, respectively.

Additionally, seasonal average bias was computed across model simulations for the Sierra Nevada (Table 3). VR-CESM 0.25° (rough) had the smallest average seasonal bias to the reanalysis dataset average with a slight negative bias of -2.7 mm, with VR-CESM 0.125° the next closest at -6.4 mm. Although WRF-9 showed best agreement with the NLDAS reanalysis datasets. The WRF and UNIFORM CESM simulations had similar tendencies to one another with a positive seasonal bias occurring in the higher resolution simulations and a negative trend in the coarser resolution simulations, much the same as Caldwell (2010) indicated for winter precipitation tendencies in California. Figure 7 shows the average climatological difference in snow water equivalent between model and reanalysis datasets. Bluer (redder) colors represent a more positive (negative) model bias over the simulation period. In general, higher resolution models tend to overproduce SWE whereas lower resolution models tend to underproduce SWE. This is likely due to the underrepresentation of topography within the model simulations. Interestingly, in several of the simulations a positive bias appears on the western slopes of the Sierra Nevada and a negative bias occurs on the eastern slopes. This may be caused by an oversensitivity to orographically forced upslope winds that push the model to overproduce snowfall as the storms move from the windward to leeward side of the Sierra Nevada. In addition, increased topographic height that does not preserve the fractal peaks and valleys in more detailed representations (see ETOPO2v2 in Figure 2) could artificially enhance orographic uplift. For example, in Figure 7 the orographic uplift bias was shown in the northern Sierra Nevada for VR-CESM 0.125° and less so in VR-CESM 0.25° (rough), a potential reason why nominal improvement was seen in snowpack characteristics for the Sierra Nevada when VR-CESM model resolution was increased.

Climatology of Total Snowpack over the Water Year

The mean daily climatological total SWE (in kg) within the Sierra Nevada was calculated in order to characterize the total water content of the region provided by snowpack (Figure 8). By averaging the total SWE each day over all years (1980-2005) and then multiplying by the area of the mask (53,102,699,313 m^2), the average snowpack mass is shown for the Sierra Nevada across model and reference datasets. Each of the datasets were grouped according to their comparable resolution counterparts (i.e., a) 0.125° (14km), b) 0.25° (28km), and c) 1° (111km)) to better showcase relative magnitudes of Sierra Nevada SWE found within a given climatological day. It should be noted that DAYMET has biases introduced during the dataset formulation that impacts its overall ability to characterize mid-season snowpack and thus alters the SCD and timing of snowmelt. Further, the CAL-ADAPT datasets were not used because daily resolution outputs were not available (only monthly and annual) and the first hour (00 or 12:00 am) of each day within the NLDAS datasets were used within the analysis. In general, VR-CESM 0.125° and VR-CESM 0.25° (rough) appear to most closely match all of the reanalysis datasets in relative magnitude (Figure 8). A bimodal profile in VR-CESM 0.125° is likely indicative of the artificial 1,000 mm cap in SWE imposed within CLM4.0 to prevent excessive snow accumulation over Antarctica - future simulations will attempt to alleviate this by removing the cap away from the polar regions. WRF-9, remapped to 14km, had a high bias associated with total SWE in the Sierra Nevada, with a SCD value of around 21.4 x 10^{12} kg (more than twice the value shown in most of the reanalysis datasets as well as VR-CESM 0.125°). In the 28km datasets, the magnitude of total SWE is consistent with the 14km results. VR-CESM 0.25° (rough) matched most closely to the NLDAS VIC 0.25° reanalysis dataset at 8.0 x 10^{12} kg, with all other datasets falling under that mark (<6.0 x 10^{12} kg). The 111km resolution datasets differed greatly from one another, with the peak accumulation of CESM-SE 1° values falling much further below the remapped reanalysis datasets. This further highlights the inability of standard-practice 1° GCM simulations to capture Sierra Nevada snowpack characteristics, especially with respect to total water content.

Snowpack Timing and Melting Patterns

Peak timing of western USA snowpack accumulation (or SCD) is traditionally thought to occur around April 1st (water day 182), although this has shifted due to regional warming trends in the western USA (Kapnick and Hall 2012; Montoya et al. 2014). Since most of the reanalysis datasets had discrepancies in representing the total water content and SCD within the Sierra Nevada, normalized values of average climate day SWE are shown in Figure 9 for all datasets in comparison to 19 SNOTEL stations (Figure 3). These stations were chosen based on daily observation availability spanning the years 1980-2005. Further, the SNOTEL locations are representative of several elevations found within the Sierra Nevada, spanning from 1864 m (Spratt Creek) to 2879 m (Virginia Lakes Ridge). Of note, the SNOTEL stations are clustered in the northern to central Sierra Nevada, with no stations present in the south. As such, a subregion of the Sierra Nevada was made to compare model results with observations from SNOTEL stations (see solid black subregion in Figure 3). This subregion was created using 12 of the USGS Hydrologic Units in the Sierra Nevada (Seaber et al. 1987). If a SNOTEL station was located within or near an adjoining hydrologic unit then the entire unit was kept (within the boundary of the Sierra Nevada Ecoregion). Further, since the lowest elevation SNOTEL station was located at 1864 m (Spratt Creek), a topographical threshold of 1824 m was imposed to create the subregion (this altitude was chosen to provide a buffer around Spratt Creek). The normalizations were computed by removing the relative mean from all climatological days within a given dataset and then dividing the resultant values by the standard deviation. Like the plots for the mean daily climatological sums of SWE, all datasets are grouped according to resolution, with added comparison to SNOTEL in each plot (Figure 9). Among models, VR-CESM 0.125° and WRF-9 matched most closely to SNOTEL. However, both had an early SCD bias. The SCD in VR-CESM 0.125° falls around water year day 170 (March 21st), the closest match to SNOTEL across all model datasets. SCD for WRF-9 falls around water year day 160 (March 11th), around two weeks before the expected date. Melt rate and the date at which the complete melt of SWE occurs differentiated VR-CESM 0.125° and WRF-9, with WRF-9 more closely matching SNOTEL. The melt rate in VR-CESM 0.125° was too rapid resulting in a complete melt occuring around 30 days sooner than in the SNOTEL dataset. DAYMET had a late SCD around day 191 (April 10th), 10 days after SNOTEL. The melt rate in the DAYMET dataset was much slower than all other datasets. Further, since DAYMET analyzed each year in isolation, the snowpack was discontinuous at water year day 91 (Thornton et al. 2014). Snowpack accumulation onset matched fairly well across all datasets, with the onset date around water year day 36 (November 5th). Within the 28km simulations, most model datasets seem to match in terms of having an earlier expected SCD clustered on water year day 151 (March 1st), around 30 days sooner than SNOTEL. The remapped version of DAYMET at 0.25° showed a similar late SCD bias (water year day 191) and showed a more drastic slow down in melt rate. All 0.25° datasets matched fairly well in snowmelt rate and accumulation onset, matching well with SNOTEL. Full melt generally occured earlier (water year day 240) across models compared to SNOTEL (water year day 270). In the 1° datasets, CESM-SE 1° had a physically unreasonable SCD (water year day 90), snowmelt rate, and accumulation onset date. Interestingly, at the 1° resolution, the biases in DAYMET are minimized and the SCD, snowmelt rate, date of complete melt, and accumulation onset date all are well within the range of SNOTEL.

Linear Trends in DJF Seasonal Snowpack

Figure 10 highlights the linear trend in DJF seasonal mean SWE values for the historical period in the Sierra Nevada SNOTEL subregion. For comparison, the 19 SNOTEL station datasets are plotted in the upper left panel. The gray lines indicate individual SNOTEL stations with the mean SNOTEL station seasonal trend shown in black and the linear trend line in red. Each of the model and reanalysis datasets are plotted using similar axis bounds, except for WRF-9 which exhibited larger values of SWE. SNOTEL stations are plotted with a larger axis, representative of these observations being pointwise measurements in regions of greater snow accumulation. The general trend across VR-CESM simulations is a slight decrease in DJF seasonal mean SWE. VR-CESM 0.125° had the largest negative trend at -0.198 mm/year, with VR-CESM 0.25° (smooth) at -0.093 mm/year and VR-CESM 0.25° (rough) at -0.029 mm/year. Except when compared to CAL-ADAPT which shows a dramatic increase in SWE and DAYMET which shows a faster decrease in SWE, the general trend for VR-CESM datasets are slightly more negative than the SNOTEL and NLDAS reanalysis datasets. This result is corroborated by Mote et al. (2005) who found a 2.2% decline in mean April 1st SWE across the in situ snowpack observational stations within the Sierra Nevada over the historical record (i.e., 1990-1997 (final period) minus 1945-1950 (initial period)), with inclusion of snow course data too. Interestingly, the 19 sampled SNOTEL stations showed a nearly flat trend (0.016 mm/year) in DJF mean seasonal SWE over the study period. WRF simulations showed differing results, with WRF-9 showing an exceedingly strong positive trend (0.410 mm/year) in mean seasonal SWE and WRF-27 having a stagnant to slightly positive trend (0.011 mm/year) matching most closely with SNOTEL. CESM-SE 1° and CESM-FV 0.25° both had a negative trend in mean seasonal SWE, with magnitudes of -0.259 mm/year and -0.200 mm/year.

Snow Cover (SNOWC) Summary Statistics

Figure 11 represents average climatological DJF SNOWC plotted for all datasets over California. Similar to SWE, an increase in resolution results in a much more heterogeneous representation of SNOWC properties that is more closely matched to observations, indicated by 12 seasons of MODIS (MODIS-5) data. A topographic influence is clearly seen as resolution is increased, with higher resolution models capturing lower elevation basins that are otherwise smoothed out. This resolution dependence manifests itself in statistical calculations of average DJF SNOWC within the Sierra Nevada (Table 4). WRF-9 showed the closest match to mean seasonal SNOWC with a value only 1.5% lower than the MODIS dataset. VR-CESM 0.25° (rough) and VR-CESM 0.125° were the next closest with a slightly more conservative estimate (7% below MODIS) of SNOWC. All other datasets, except CESM-FV 0.25° which had a positive bias of around 8%, had much smaller estimates of mean seasonal SNOWC. CESM-SE 1° provided the largest underestimate among the model datasets with mean seasonal values at a quarter of the comparable remapped version of MODIS. Interestingly, two of the best available high resolution reanalysis datasets (NCEP and NARR) seem unable to properly capture the Sierra Nevada SNOWC characteristics in the MODIS dataset, with most of the reanalysis datasets showing a negative bias for SNOWC. NARR-32 and NCEP-35 had mean SNOWC values at half to two-thirds of the value indicated by MODIS and NLDAS VIC, NOAH, and MOSAIC were at 84%, 74%, and 47% of MODIS, respectively. The median values for DJF SNOWC for VR-CESM 0.125° and VR-CESM 0.25° showed a close approximation to those seen in NLDAS VIC. As expected, since SNOWC is capped at 100%, maximum DJF SNOWC was reached by most modeling platforms.

Seasonal Variability in Snow Cover

Mean seasonal variability (interannual standard deviation of the seasonal mean) in SNOWC is shown over California (Figure 12). Standard deviation values for each of the simulations are given in Table 4. As with the mean seasonal SNOWC values, WRF-9 had the best representation of seasonal variability within the Sierra Nevada, with a close approximation to standard deviation values in the remapped MODIS dataset (although it underestimates standard deviation in the lee of the

Sierra Nevada). VR-CESM 0.25° (rough) also was able to characterize seasonal variability at a realistic level, with a standard deviation only 14% below MODIS. All other modeling platforms had a conservative estimate of variability ranging from half to three-fourths of the observed standard deviation, when comparing to common remapped resolutions. This result is apparent in Figure 13 for each dataset and analyzing the IQRs. All datasets, save for WRF-9 and CESM-FV 0.25°, had a conservative estimate of SNOWC summary statistics when compared to MODIS. Median values, along with IQRs, are too low with a noticeable bias in the 75th percentiles.

Pattern Correlation and Bias in Snow Cover

The average seasonal centered Pearson product-moment coefficients and mean climatological bias for SNOWC are exhibited in Table 5. MODIS was not used in the centered Pearson calculations as it only spanned five years of the historical period (2000-2005). A close match was seen across both VR-CESM and WRF modeling platforms when compared to the three NLDAS datasets. Most values fell around 0.74 for the VR-CESM simulations and 0.84 for the WRF simulations. The CESM-FV and CESM-SE had the lowest correlations at 0.53 and 0.15, respectively. The smallest mean climatological bias in DJF SNOWC between MODIS and the model datasets was VR-CESM 0.125°, VR-CESM 0.25° (rough) and WRF-27, with negative baises of approximately 6-7%. CESM-SE 1° produced the worst match across model datasets with a -28.5% bias. Of note, the NLDAS reanalysis datasets also widely varied in their ability to characterize mean climatological SNOWC bias when compared to MODIS with consistent negative biases ranging between -9.2% (NLDAS VIC) to -29.4% (NLDAS MOSAIC).

5. Discussion and Conclusion

The primary goal of this paper has been to assess the efficacy of VR-CESM in simulating the mean climatological state and seasonal variability within Sierra Nevada snowpack metrics (i.e., SWE, SCD, and SNOWC). It was determined that the efficacy of the VR-CESM framework in simulating climatological mean and seasonal variability in both SWE and SNOWC was competitive with traditional dynamical downscaling. Overall, considering California's complex terrain and intermittent climate, a 0.68 centered correlation (less correlated, yet similar to values seen in WRF), negative mean SWE bias of $<$7 mm, and an IQR well within the range of values exhibited in the best available spatially continuous datasets for SWE, the ability of both VR-CESM 0.25° (rough) and VR-CESM 0.125° to simulate SWE on both climatological and seasonal scales was confirmed. Of note, both of the VR-CESM simulations were solely constrained by prescribed SST and sea ice data, whereas WRF simulations were further constrained at lateral boundaries by ERA-interim data (in addition to SST and sea ice), yet both showed comparable statistical properties. This was similarly confirmed for the climatological mean for DJF SNOWC where both the VR-CESM 0.125° and VR-CESM 0.25° (rough) simulations were within 7% of the expected mean MODIS value. VR-CESM 0.25° (rough) was able to characterize MODIS' standard deviation well (86% match). WRF-9 had the best representation of SNOWC with a near identical representation in mean, standard deviation, and IQR, compared to MODIS, but at the cost of unreasonably high SWE values. This is likely indicative of the over-exaggeration of topography at higher resolutions in the model, where the fractal nature of peaks and, importantly, valleys are misrepresented (compare ETOPO2v2 to model topography in Figure 2) leading to a bias in overall snowpack characterizations. VR-CESM, as well as WRF, conveyed mixed results in representing seasonal variability in SWE (average standard deviation value at each grid point), with generally conservative estimates across all assessed modeling platforms except WRF-9 and CESM-FV 0.25° which had much higher estimates. The total water content of snowpack within the Sierra Nevada was best represented in both VR-CESM 0.125° and VR-CESM 0.25° (rough) when compared to the remapped NLDAS VIC reference dataset at their respective resolutions. VR-CESM 0.125° and WRF-9 showcased the best representation, across datasets, of SCD timing, snowmelt rate, and snowpack accumulation onset, in comparison to SNOTEL. The two datasets differed in the date at which complete melting of SWE occured with VR-CESM 0.125° occuring too early, whereas WRF-9 had a slightly late onset. Interestingly, both SWE and SNOWC didn't show a significant enhancement in snowpack properties when VR-CESM resolution was moved from 0.25° to 0.125°; in fact the 0.25° simulation (VR-CESM 0.25° (rough)) was slightly more skillful when considering all metrics. Topographical roughness was found to play a much more significant role in representing snowpack properties with VR-CESM 0.25° (rough) seeing a sixteen-fold decrease in average seasonal SWE bias, threefold increase in SWE seasonal variability, an IQR increase from 48.9 to 64.1, and a considerable increase in the SCD total water content for the Sierra Nevada. This is an improvement when compared to the average of all of the reanalysis datasets. Furthermore, DJF temperature characteristics may have played a role in modulating which of the simulations performed most optimally. Figure 14 highlights average climatological DJF 2m surface temperatures for only the model simulations. Below freezing (< 273 K) temperatures are shown to be maintained over greater areas for the climatic period across all higher resolution ($\leq 0.25°$) simulations, likely because of increased topographic elevations in those areas. This temperature maintenance likely drives winter season snowpack accumulation and sustainment.

The VR-CESM framework provides greatly enhanced representation of snowpack properties compared to widely used GCMs (i.e., CESM-FV 1° and CESM-FV 0.25°). Simulation of Sierra Nevada snowpack in the VR-CESM framework is competitive with traditional dynamical downscaling techniques, but has the additional means of providing dynamic interaction with large-scale atmosphere-ocean drivers and teleconnections that might not otherwise manifest in an RCM constrained by boundary conditions. These two points lend them themselves well to using certain versions of VR-CESMs (namely VR-CESM 0.25° (rough) and VR-CESM 0.125°) in projecting future climate change scenarios and their resultant impacts on water resources over the western USA.

The topographical smoothing between the two VR-CESM 0.25° simulations had the most dramatic influence on snowpack product tendencies found within the VR-CESM framework, even when compared to changes resulting from a doubling of model resolution from 0.25° to 0.125°. As shown in Table 2, mean seasonal SWE for the Sierra Nevada nearly doubled from 50.4 mm to 95.2 mm between VR-CESM 0.25° (smooth) and VR-CESM 0.25° (rough), with a decrease in average DJF climate bias in SWE from -52% to -2.3% when compared to the reanalysis dataset average. This tendency was similar for the lower quartile, median, and higher quartile values. Similarly, the seasonal variability, indicated by the standard deviation plots (Figure 5) and standard deviation values in Table 2, nearly tripled, making the VR-CESM 0.25° (rough) simulation the closest match to the reanalysis dataset average within all model simulations. Changes in SNOWC trends were also apparent, although less dramatic than SWE (Table 4). Average seasonal SNOWC increased by 9% and the IQR increased from 48.9 to 64.1, matching more closely to the MODIS dataset value of 74.5, with the higher quartile less conservatively biased.

Improved topographical resolution also resulted in better representation of the snow characteristics of the maritime mountain ranges (e.g., the Cascades and the Coastal Range) (Figure 4). Maritime mountain ranges have shown some of the greatest snowpack decreases over the historical record (Serreze et al. (1999); Mote (2003); Mote et al. (2005)) and are in need of the best available climate change impact analysis due to a greater susceptibility to climate change trends (i.e., warmer and potentially more precipitous weather fronts originating from relatively warmer ocean waters). This is important because conventional GCM simulations are generally performed at resolutions too coarse to properly resolve the aforementioned topographical forcings and, thus, may bias evaluations used to guide climate impact studies and climate policy formulation. This isn't to say that the VR-CESM framework provides perfect representation of these ranges, but that it provides a more realistic and computationally effective means to characterize these ranges in a changing climate. This subject will be the target of further research.

A higher resolution surface dataset for PFT type would have been beneficial for this study, to capitalize on the higher resolution ($<0.5°$) VR-CESM grids implemented into CLM, however none were available at the time of writing. An extensive review of the North American and European snowpack-canopy interaction literature by Varhola et al. (2010) argued that snowpack accumulation and melting patterns can be significantly altered by changes in forest cover, accounting for relative variance changes of 57% in snow accumulation and 72% in snow ablation. After discussion with the CLM development team at NCAR, a two minute PFT dataset for the year 2000 was identified. This dataset will be used in future simulations to assess the effects of canopy interactions on snowpack metrics within a VR-CESM framework.

Added benefits of the VR-CESM framework, not discussed previously, include the large enhancement in computational efficiency. For example, the 0.25°(0.125°) VR-CESM grid had approximately 8,400 (11,300) elements. When compared to conventional uniform resolution grids at 1.00°, 0.25° or 0.125°, which have 5,400, 86,400, and 345,600 elements respectively, a theoretical speedup in computation time of 10 to 30 times is expected for the VR-CESM framework, with the assumption of linear computational scalability highlighted in Dennis et al. (2011) and Zarzycki et al. (2014a). Therefore, for a relatively similar computational cost of a uniform 1.00° grid, one can get vastly improved snowpack product characteristics over a limited region of interest, especially within the California Sierra Nevada. This is a function of not only resolving smaller scale meteorological features, but also due to better representations of topography and, in some cases, land surface properties. Therefore, for only a fraction of the cost of a high resolution uniform GCM run, the VR-CESM approach can be performed on a local server ($<$1000 processors), with 20-40 day turnarounds on 25 year simulation periods, and provide model resolutions of 0.25° (28 km) to 0.125° (14 km), which decision makers (especially in the western USA water sector), may find more useful in regional planning endeavors. The enhanced representation of snowpack and relative computational efficiency of VR-CESM lends itself well to future investigations of other SWE dependent regions of the western USA, as well as ensemble-based climate change scenario analysis.

Acknowledgments. The authors would like to acknowledge the computational support, and patience, provided by the University of California, Davis Farm Cluster IT support team (i.e., Bill Broadley and Terri Knight). Additionally, we would like to thank all reviewers for their helpful comments. We believe the quality of the manuscript is greatly improved after incorporating their suggestions. Further, the fruitful conversations with Alison Whipple, Dustin Grogan and Nicolas Bambach throughout the production of this paper were indispensable and truly appreciated. This research was funded by the National Science Foundation (NSF) via the Climate Change, Water, and Society Integrated Graduate Education and Research Traineeship (IGERT) program at the University of California, Davis (NSF Award Number: 1069333), the Leland Roy Saxon and Georgia Wood Saxon Fellowship, and the Department of Energy, Office of Science project "Multiscale Methods for Accurate, Efficient, and Scale-Aware Models of the Earth System."

References

Anderson, E. A., 1976: A point of energy and mass balance model of snow cover. *NOAA Tech. Rep. NWS*, **19**, 1–150.

Bales, R. C., J. J. Battles, Y. Chen, M. H. Conklin, E. Holst, K. L. OHara, P. Saksa, and W. Stewart, 2011: Forests and water in the sierra nevada: Sierra nevada watershed ecosystem enhancement project. *Sierra Nevada Research Institute report*, **(11.1)**.

Bales, R. C., N. P. Molotch, T. H. Painter, M. D. Dettinger, R. Rice, and J. Dozier, 2006: Mountain hydrology of the western United States. *Water Resources Research*, **42**, W08 432.

Caldwell, P., 2010: California Wintertime Precipitation Bias in Regional and Global Climate Models. *Journal of Applied Meteorology and Climatology*, **49**, 2147–2158.

Cayan, D. R., 1996: Interannual climate variability and snowpack in the western United States. *Journal of Climate*, **9**, 928–948.

Cayan, D. R., K. T. Redmond, and L. G. Riddle, 1999: ENSO and Hydrologic Extremes in the Western United States. *Journal of Climate*, **12**, 2881–2893.

Chen, F., and J. Dudhia, 2001: Coupling an advanced land surface-hydrology model with the Penn State-NCAR MM5 modeling system. Part I: Model implementation and sensitivity. *Monthly Weather Review*, **129 (4)**, 569–585.

Collins, W. D., and Coauthors, 2004: Description of the NCAR community atmosphere model (CAM 3.0). Tech. rep., Tech. Rep. NCAR/TN-464+ STR.

Dee, D., and Coauthors, 2011: The ERA-Interim reanalysis: Configuration and performance of the data assimilation system. *Quarterly Journal of the Royal Meteorological Society*, **137 (656)**, 553–597.

DeFlorio, M. J., D. W. Pierce, D. R. Cayan, and A. J. Miller, 2013: Western US extreme precipitation events and their relation to ENSO and PDO in CCSM4. *Journal of Climate*, **26 (12)**, 4231–4243.

Dennis, J., and Coauthors, 2011: CAM-SE: A scalable spectral element dynamical core for the Community Atmosphere Model. *International Journal of High Performance Computing Applications*, 1094342011428142.

Dettinger, M., 2011: Climate Change, Atmospheric Rivers, and Floods in California - A Multimodel Analysis of Storm Frequency and Magnitude Changes. *JAWRA Journal of the American Water Resources Association*, **47**, 514–523.

Dettinger, M. D., D. R. Cayan, H. F. Diaz, and D. M. Meko, 1998: North-south precipitation patterns in western North America on interannual-to-decadal timescales. *Journal of Climate*, **11**, 3095–3111.

Dettinger, M. D., F. M. Ralph, T. Das, P. J. Neiman, and D. R. Cayan, 2011: Atmospheric rivers, floods and the water resources of California. *Water*, **3 (2)**, 445–478.

Fang, C., L. Wu, and X. Zhang, 2014: The impact of global warming on the pacific decadal oscillation and the possible mechanism. *Advances in Atmospheric Sciences*, **31**, 118–130.

Gates, W. L., 1992: AMIP: The atmospheric model intercomparison project. *Bulletin of the American Meteorological Society*, **73 (12)**, 1962–1970.

Ghan, S. J., X. Liu, R. C. Easter, R. Zaveri, P. J. Rasch, J.-H. Yoon, and B. Eaton, 2012: Toward a minimal representation of aerosols in climate models: Comparative decomposition of aerosol direct, semidirect, and indirect radiative forcing. *Journal of Climate*, **25 (19)**, 6461–6476.

Gimeno, L., R. Nieto, M. Vázquez, and D. A. Lavers, 2014: Atmospheric rivers: a mini-review. *Atmospheric Science*, **2**, 2.

Glantz, M. H., R. W. Katz, and N. Nicholls, 1991: *Teleconnections linking worldwide climate anomalies*. Cambridge University Press, 284–308 pp.

Guan, B., N. P. Molotch, D. E. Waliser, E. J. Fetzer, and P. J. Neiman, 2010: Extreme snowfall events linked to atmospheric rivers and surface air temperature via satellite measurements. *Geophysical Research Letters*, **37 (20)**.

Guan, B., N. P. Molotch, D. E. Waliser, E. J. Fetzer, and P. J. Neiman, 2013: The 2010/2011 snow season in California's Sierra Nevada: Role of atmospheric rivers and modes of large-scale variability. *Water Resources Research*, **49**, 6731–6743.

Hall, D. K., and G. A. Riggs, 2007: Accuracy assessment of the MODIS snow products. *Hydrological Processes*, **21 (12)**, 1534–1547.

Hall, D. K., G. A. Riggs, and V. V. Salomonson, 2006: Modis snow and sea ice products. *Earth science satellite remote sensing*, Springer, 154–181.

Hanak, E., and J. R. Lund, 2012: Adapting californias water management to climate change. *Climatic Change*, **111 (1)**, 17–44.

Hong, S.-Y., and J.-O. J. Lim, 2006: The WRF single-moment 6-class microphysics scheme (WSM6). *Asia-Pacific Journal of Atmospheric Sciences*, **42 (2)**, 129–151.

Hong, S.-Y., Y. Noh, and J. Dudhia, 2006: A new vertical diffusion package with an explicit treatment of entrainment processes. *Monthly Weather Review*, **134 (9)**, 2318–2341.

Huang, X., A. M. Rhoades, P. A. Ullrich, and C. M. Zarzycki, 2015: High-resolution regional climate model evaluation using variable-resolution CESM over California. *Submitted to Journal of Climate*.

Iacono, M. J., J. S. Delamere, E. J. Mlawer, M. W. Shephard, S. A. Clough, and W. D. Collins, 2008: Radiative forcing by long-lived greenhouse gases: Calculations with the AER radiative transfer models. *Journal of Geophysical Research: Atmospheres (1984–2012)*, **113 (D13)**.

Jordan, R., 1991: A one-dimensional temperature model for a snow cover: Technical documentation for SNTHERM. 89. Tech. rep., DTIC Document.

Kain, J. S., 2004: The Kain-Fritsch convective parameterization: an update. *Journal of Applied Meteorology*, **43 (1)**, 170–181.

Kapnick, S., and A. Hall, 2012: Causes of recent changes in western North American snowpack. *Climate Dynamics*, **38**, 1885–1899.

Lawrence, D. M., and Coauthors, 2011: Parameterization improvements and functional and structural advances in version 4 of the Community Land Model. *Journal of Advances in Modeling Earth Systems*, **3**.

Li, W., and C. E. Forest, 2014: Estimating the sensitivity of the atmospheric teleconnection patterns to SST anomalies using a linear statistical method. *Journal of Climate*, **27 (24)**, 9065–9081.

Maurer, E. P., and H. G. Hidalgo, 2008: Utility of daily vs. monthly large-scale climate data: an intercomparison of two statistical downscaling methods. *Hydrology and Earth System Sciences*, **12 (2)**, 551–563, doi:10.5194/hess-12-551-2008, URL http://www.hydrol-earth-syst-sci.net/12/551/2008/.

Mesinger, F., and Coauthors, 2006: North American Regional Reanalysis. *Bulletin of the American Meteorological Society*, **87**, 343–360.

Montoya, E., J. Dozier, and W. Meiring, 2014: Biases of April 1 snow water equivalent records in the Sierra Nevada and their associations with large-scale climate indices. *Geophysical Research Letters*, **41 (16)**, 5912–5918.

Morrison, H., and A. Gettelman, 2008: A new two-moment bulk stratiform cloud microphysics scheme in the Community Atmosphere Model, version 3 (CAM3). Part I: Description and numerical tests. *Journal of Climate*, **21 (15)**, 3642–3659.

Mote, P. W., 2003: Trends in snow water equivalent in the Pacific Northwest and their climatic causes. *Geophysical Research Letters*, **30 (12)**.

Mote, P. W., A. F. Hamlet, M. P. Clark, and D. P. Lettenmaier, 2005: Declining mountain snowpack in Western North America. *Bulletin of the American Meteorological Society*, **86**, 39–49.

National Geophysical Data Center, 2006: 2-minute Gridded Global Relief Data (ETOPO2) v2. National Geophysical Data Center, NOAA. . Doi:10.7289/V5J1012Q [2014].

Neale, R. B., J. H. Richter, and M. Jochum, 2008: The impact of convection on ENSO: From a delayed oscillator to a series of events. *Journal of Climate*, **21 (22)**, 5904–5924.

Neale, R. B., and Coauthors, 2010: Description of the NCAR Community Atmosphere Model (CAM 5.0). NCAR Technical Note NCAR/TN-486+STR, National Center for Atmospheric Research, Boulder, Colorado, 268 pp.

Oleson, K., and Coauthors, 2010: Technical Description of version 4.0 of the Community Land Model (CLM). NCAR Technical Note NCAR/TN-478+STR, National Center for Atmospheric Research, Boulder, Colorado, 257 pp. doi:10.5065/D6FB50WZ.

Palmer, P. L., 1988: The scs snow survey water supply forecasting program: Current operations and future directions. *Proceedings Western Snow Conference*, 43–51.

Pandey, G. R., D. R. Cayan, and K. P. Georgakakos, 1999: Precipitation structure in the Sierra Nevada of California during winter. *Journal of Geophysical Research: Atmospheres (1984–2012)*, **104 (D10)**, 12 019–12 030.

Park, S., and C. S. Bretherton, 2009: The University of Washington shallow convection and moist turbulence schemes and their impact on climate simulations with the Community Atmosphere Model. *Journal of Climate*, **22 (12)**, 3449–3469.

Park, S., C. S. Bretherton, and P. J. Rasch, 2014: Integrating cloud processes in the Community Atmosphere Model, Version 5. *Journal of Climate*, **27 (18)**, 6821–6856.

Pierce, D. W., and D. R. Cayan, 2013: The uneven response of different snow measures to human-induced climate warming. *Journal of Climate*, **26**, 4148–4167.

Ralph, F. M., P. J. Neiman, and G. A. Wick, 2004: Satellite and CALJET aircraft observations of atmospheric rivers over the eastern North Pacific Ocean during the winter of 1997/98. *Monthly Weather Review*, **132 (7)**, 1721–1745.

Rupp, D. E., P. W. Mote, N. L. Bindoff, P. A. Stott, and D. A. Robinson, 2013: Detection and attribution of observed changes in Northern Hemisphere spring snow cover. *Journal of Climate*, **26**, 6904–6914.

Saha, S., and Coauthors, 2014: The NCEP climate forecast system version 2. *Journal of Climate*, **27 (6)**, 2185–2208.

Salzmann, N., and L. O. Mearns, 2012: Assessing the performance of multiple regional climate model simulations for seasonal mountain snow in the upper Colorado River basin. *Journal of Hydrometeorology*, **13**, 539–556.

Seaber, P. R., F. P. Kapinos, and G. L. Knapp, 1987: *Hydrologic unit maps*. US Government Printing Office.

Serreze, M. C., M. P. Clark, R. L. Armstrong, D. A. McGinnis, and R. S. Pulwarty, 1999: Characteristics of the western United States snowpack from snowpack telemetry (SNOTEL) data. *Water Resources Research*, **35 (7)**, 2145–2160.

Stewart, W. C., 1996: Economic assessment of the ecosystem. *Sierra Nevada ecosystem project: final report to Congress*, Citeseer, Vol. 3, 973–1064.

Tanaka, S. K., and Coauthors, 2006: Climate warming and water management adaptation for california. *Climatic Change*, **76 (3-4)**, 361–387.

Taylor, M., J. Tribbia, and M. Iskandarani, 1997: The Spectral Element Method for the Shallow Water Equations on the Sphere. *Journal of Computational Physics*, **130**, 92–108.

Taylor, M. A., and A. Fournier, 2010: A compatible and conservative spectral element method on unstructured grids. *Journal of Computational Physics*, **229 (17)**, 5879–5895.

Thornton, P., M. Thornton, B. Mayer, N. Wilhelmi, Y. Wei, R. Devarakonda, and R. Cook, 2014: Daymet: Daily Surface Weather Data on a 1-km Grid for North America, Version 2. Data set. Available on-line [http://daac. ornl. gov] from Oak Ridge National Laboratory Distributed Active Archive Center, Oak Ridge, Tennessee, USA. Date accessed: 2014/11/01. Temporal range: 1980-2005. Tech. rep., http://dx. doi. org/10.3334/ORNLDAAC/1219.

Ullrich, 2014: SQuadGen: Spherical Quadrilateral Grid Generator. [Available online at http://climate.ucdavis.edu/squadgen.php].

Ullrich, P. A., and M. A. Taylor, 2015: Arbitrary-Order Conservative and Consistent Remapping and a Theory of Linear Maps, Part 1. *Monthly Weather Review*, **(2015)**.

Varhola, A., N. C. Coops, M. Weiler, and R. D. Moore, 2010: Forest canopy effects on snow accumulation and ablation: An integrative review of empirical results. *Journal of Hydrology*, **392 (3)**, 219–233.

Wallace, J. M., and D. S. Gutzler, 1981: Teleconnections in the geopotential height field during the Northern Hemisphere winter. *Monthly Weather Review*, **109 (4)**, 784–812.

Wang, S.-Y., L. Hipps, R. R. Gillies, and J.-H. Yoon, 2014: Probable causes of the abnormal ridge accompanying the 2013–2014 California drought: ENSO precursor and anthropogenic warming footprint. *Geophysical Research Letters*, **41 (9)**, 3220–3226.

Wehner, M. F., and Coauthors, 2014: The effect of horizontal resolution on simulation quality in the Community Atmospheric Model, CAM5. 1. *Journal of Advances in Modeling Earth Systems*.

Wise, E. K., 2012: Hydroclimatology of the US Intermountain West. *Progress in Physical Geography*, **36**, 458–479.

Xia, Y., and Coauthors, 2012a: Continental-scale water and energy flux analysis and validation for North American Land Data Assimilation System project phase 2 (NLDAS-2): 2. Validation of model-simulated streamflow. *Journal of Geophysical Research: Atmospheres (1984–2012)*, **117 (D3)**.

Xia, Y., and Coauthors, 2012b: Continental-scale water and energy flux analysis and validation for the North American Land Data Assimilation System project phase 2 (NLDAS-2): 1. Intercomparison and application of model products. *Journal of Geophysical Research: Atmospheres (1984–2012)*, **117 (D3)**.

Yang, Z.-L. Y., X. Cai, G. Zhang, A. A. Tavakoly, Q. Jin, L. H. Meyer, and X. Guan, 2011: Technical Description of the Community Noah Land Surface Model with Multi-Paramterization Options (Noah-MP). Tech. rep., Center for Integrated Earth System Science, The University of Texas at Austin, Boulder, Colorado, 1-72 pp.

Yen, Y.-C., 1965: Heat transfer characteristics of naturally compacted snow. Tech. rep., DTIC Document.

Yongjiu, D., and Z. Qingcun, 1997: A land surface model (IAP94) for climate studies part I: formulation and validation in off-line experiments. *Advances in Atmospheric Sciences*, **14**, 433–460.

Zarzycki, C. M., and C. Jablonowski, 2014: A multidecadal simulation of Atlantic tropical cyclones using a variable-resolution global atmospheric general circulation model. *Journal of Advances in Modeling Earth Systems*.

Zarzycki, C. M., C. Jablonowski, and M. A. Taylor, 2014a: Using Variable Resolution Meshes to Model Tropical Cyclones in the Community Atmosphere Model. *Monthly Weather Review*, **142 (3)**, 1221–1239, doi:10.1175/MWR-D-13-00179.1.

Zarzycki, C. M., C. Jablonowski, D. R. Thatcher, and M. A. Taylor, 2015: Effects of Localized Grid Refinement on the General Circulation and Climatology in the Community Atmosphere Model. *Journal of Climate*, **28**, 2777–2803.

Zarzycki, C. M., M. N. Levy, C. Jablonowski, J. R. Overfelt, M. A. Taylor, and P. A. Ullrich, 2014b: Aquaplanet Experiments Using CAM's Variable-Resolution Dynamical Core. *Journal of Climate*, **27**, 5481–5503, doi:10.1175/JCLI-D-14-00004.1.

TABLE 1. Datasets, and associated metadata, used to analyze the accuracy of the Variable Resolution Global Climate Model (VR-CESM) simulations

Datasets	*Snowpack Product*	*Spatial Resolution*	*Temporal Resolution*	*Projection*	*Years Assessed*
VR-CESM 0.25° (smooth)	SWE and SNOWC	28km	Daily	VR-CESM in CAM and CLM - Equidistant	1980-2005
VR-CESM 0.25° (rough)	SWE and SNOWC	28km	Daily	VR-CESM in CAM and CLM - Equidistant	1980-2005
VR-CESM 0.125°	SWE and SNOWC	14km	Daily	VR-CESM in CAM and CLM - Equidistant	1980-2005
UNIFORM CESM (SE and FV)	SWE and SNOWC	111 km and 28 km	Daily	Equidistant	1980-2005
WRF	SWE and SNOWC	27km, 9km	Daily	Lambert Conformal	1980-2005
DAYMET	SWE	1km	Daily	Lambert Conformal Conic	1980-2005
CAL-ADAPT	SWE	14km	Monthly	Equidistant	1980-2005
SNOTEL	SWE	Point Source (19 stations)	Daily	Point Source (Automated Station)	1980-2005
NLDAS-2	SWE and SNOWC	14km	Hourly, Monthly	Equidistant	1980-2005
NCEP (CFSv2)	SWE and SNOWC	35km	Daily	Equidistant	1980-2005
NARR	SNOWC	32km	Daily	Lambert Conformal	1980-2005
MODIS/Terra	SNOWC	5km	Monthly	Geographic Lat Lon or Climate Modeling Grid (CMG)	2000-2013

TABLE 2. Summary Statistics of Seasonally Averaged Snow Water Equivalent (SWE) in the Sierra Nevada

Model	*DJF Seasons*	*Mean*	*Standard Deviation*	*Lower Quartile*	*Median*	*Upper Quartile*	*Max*	*Sierra Mask Points*
VR-CESM 0.25° (smooth)	25	50.4	80.1	3.10	19.8	60.9	663	2175
VR-CESM 0.25° (rough)	25	95.2	134	5.30	32.9	132	750	2175
VR-CESM 0.125°	25	91.0	125	7.40	37.6	125	751	8775
WRF-27	25	71.6	102	6.20	29.2	91.0	701	2175
WRF-9	22	233	365	5.60	48.8	314	3090	14058
WRF-9 (REGRID 0.125°)	22	231	349	7.60	63.2	317	2850	7721
CESM-SE 1°	25	3.40	7.50	0.00	0.50	2.40	41.7	150
CESM-FV 0.25°	25	179	188	23.6	111	291	875	2175
DAYMET	25	109	176	1.40	36.9	141	1000	1202620
DAYMET (REGRID 0.125°)	25	107	173	1.60	35.1	140	1000	8678
DAYMET (REGRID 0.25°)	25	102.3	168.4	1.90	32.0	127	1000	2156
DAYMET (REGRID 1°)	25	28.0	36.8	2.00	12.1	39.8	174	149
NLDAS VIC 0.125°	25	72.9	103	2.90	29.1	101	777	8748
NLDAS VIC (REGRID 0.25°)	25	73.8	102	3.10	29.4	105	629	2169
NLDAS VIC (REGRID 1.00°)	25	38.1	71.3	1.50	7.80	30.8	345	149
NLDAS NOAH 0.125°	25	56.3	84.2	1.50	19.7	75.5	616	8775
NLDAS NOAH (REGRID 0.25°)	25	57.4	84.4	1.70	21.1	75.9	518	2175
NLDAS NOAH (REGRID 1°)	25	28.7	56.4	0.70	5.60	23.0	321	150
NLDAS MOSAIC 0.125°	25	59.5	98.6	0.60	11.3	76.3	773	8748
NLDAS MOSAIC (REGRID 0.25°)	25	60.5	98.2	0.70	11.6	79.2	647	2171
NLDAS MOSAIC (REGRID 1°)	25	27.1	60.9	0.19	2.40	14.2	325	149
CAL-ADAPT CCSM3 0.125°	25	134	154	9.60	80.7	202	1060	8775
CAL-ADAPT CCSM3 (REGRID 0.25°)	25	136	155	9.90	80.8	206	944	2175
CAL-ADAPT CCSM3 (REGRID 1°)	25	73.4	88.1	1.20	48.4	107	416	150
CAL-ADAPT CNRM 0.125°	25	125	157	8.10	67.3	185	1210	8773
CAL-ADAPT CNRM (REGRID 0.25°)	25	127	158	8.60	68.5	191	1090	2174
CAL-ADAPT CNRM (REGRID 1°)	25	66.4	88.2	2.40	27.4	89.8	544	149
CAL-ADAPT GFDL 0.125°	25	95.0	121	5.40	49.1	141	959	8775
CAL-ADAPT GFDL (REGRID 0.25°)	25	96.3	122	5.60	49.3	141	855	2175
CAL-ADAPT GFDL (REGRID 1°)	25	47.0	65.2	1.90	26.0	67.6	448	150
CAL-ADAPT PCM1 0.125°	25	129	151	14.2	75.2	186	926	8775
CAL-ADAPT PCM1 (REGRID 0.25°)	25	131	153	15.4	75.8	188	861	2175
CAL-ADAPT PCM1 (REGRID 1°)	25	73.8	90.5	6.60	45.4	99.1	426	150
Reanalysis Dataset Average 0.125°	N/A	97.4	134	5.50	45.9	138	915	N/A
Reanalysis Dataset Average 0.25°	N/A	97.9	134	5.90	46.1	139	818	N/A
SNOTEL	25	237	186	103	195	308	1220	19 stations

TABLE 3. Snow Water Equivalent (SWE) Climatological Bias and DJF Seasonal Pearson Product-Moment Coefficients (Centered) within the Sierra Nevada. Absolute value averages are computed to eliminate sign dependency in bias comparisons across datasets.

Model	VR-CESM 0.125°	VR-CESM 0.25° (rough)	VR-CESM 0.25° (smooth)	WRF-9	WRF-27	CESM-FV 0.25°	CESM-SE 1°
DJF Climate Bias (units - mm)							
NLDAS VIC	18.1	21.4	23.4	158	2.20	106	34.7
NLDAS NOAH	34.7	37.8	7.00	175	14.2	122	25.3
NLDAS MOSAIC	31.5	34.7	10.1	172	11.1	119	23.7
CALADAPT CCSM3	42.8	40.3	85.1	97.3	63.9	43.9	70.0
CALADAPT CNRM	34.4	31.8	76.6	105.7	55.4	52.4	63.0
CALADAPT GFDL	4.00	1.10	45.9	136	24.7	83.1	43.6
CALADAPT PCM1	37.9	35.3	80.1	102	58.9	48.9	70.4
DAYMET	16.3	7.10	51.9	124	30.7	77.1	24.6
Reanalysis Dataset Absolute Value Average	27.5	26.2	47.5	134	33.8	81.3	44.5
DJF Pearson Pattern Correlation							
NLDAS VIC	0.72	0.75	0.72	0.90	0.78	0.33	0.09
NLDAS NOAH	0.69	0.71	0.68	0.88	0.74	0.35	0.07
NLDAS MOSAIC	0.68	0.73	0.69	0.86	0.73	0.25	0.06
CALADAPT CCSM3	0.71	0.75	0.75	0.85	0.75	0.32	0.32
CALADAPT CNRM	0.71	0.75	0.73	0.85	0.75	0.31	0.29
CALADAPT GFDL	0.70	0.74	0.75	0.84	0.73	0.29	0.32
CALADAPT PCM1	0.72	0.76	0.73	0.86	0.76	0.35	0.33
DAYMET	0.45	0.48	0.42	0.63	0.48	0.04	0.08
Reanalysis Dataset Average	0.67	0.71	0.68	0.83	0.71	0.28	0.19

TABLE 4. Summary Statistics of Seasonally Averaged Snow Cover (SNOWC) in the Sierra Nevada

Model	*DJF Seasons*	*Mean*	*Standard Deviation*	*Lower Quartile*	*Median*	*Upper Quartile*	*Max*	*Sierra Mask Points*
VR-CESM 0.25° (smooth)	25	40.0	30.1	13.6	36.5	62.5	100	2175
VR-CESM 0.25° (rough)	25	48.9	33.5	17.5	46.7	81.6	100	2175
VR-CESM 0.125°	25	48.7	30.3	22.0	47.8	74.1	100	2175
WRF-27	25	42.9	30.1	15.3	40.0	67.2	98.0	2175
WRF-9	22	55.0	37.3	16.3	58.6	96.7	98.0	14058
WRF-9 (REGRID 0.125°)	22	54.3	35.6	19.1	56.3	92.3	98.0	7721
CESM-SE 1°	25	9.10	12.3	0.60	4.40	11.9	60.3	150
CESM-FV 0.25°	25	62.8	32.2	36.6	69.9	92.3	100.0	2175
NCEP-35	25	37.1	25.5	15.3	33.7	56.5	96.6	1350
NARR-32	25	22.5	27.5	0.60	9.60	37.5	100	1175
MODIS-5	12	56.7	36.6	18.0	65.0	93.0	100	25932
MODIS-5 (REGRID 0.125°)	12	55.8	35.8	18.5	62.8	90.7	100	4188
MODIS-5 (REGRID 0.25°)	12	55.0	36.0	16.3	61.4	90.8	100	1032
MODIS-5 (REGRID 1°)	12	37.6	33.1	3.80	34.0	69.1	95.7	60
NLDAS VIC 0.125	25	46.6	33.0	15.0	45.9	75.9	100	8742
NLDAS VIC 0.25	25	46.8	33.3	14.9	45.1	78.4	100	2166
NLDAS VIC 1.00	25	32	25.4	11.6	26.6	45.8	87.5	149
NLDAS NOAH 0.125	25	41.5	33.8	7.60	37.5	71.6	100	8720
NLDAS NOAH 0.25	25	42.1	34.3	8.30	38.4	73.4	100	2164
NLDAS NOAH 1.00	25	25.9	25.4	4.10	18.3	40.7	85.0	149
NLDAS MOSAIC 0.125	25	26.4	29.6	1.40	13.1	45.4	98.8	8722
NLDAS MOSAIC 0.25	25	26.8	30.1	1.40	13.1	47.6	98.2	2163
NLDAS MOSAIC 1.00	25	12.8	18.8	0.30	4.20	14.4	66.7	149
Reanalysis Dataset Average 0.125°	N/A	42.6	33.1	10.6	39.8	70.9	99.7	N/A
Reanalysis Dataset Average 0.25°	N/A	42.7	33.5	10.2	39.5	72.6	99.6	N/A

TABLE 5. Snow Cover (SNOWC) Climatological Bias and DJF Seasonal Pearson Product-Moment Coefficients (Centered) within the Sierra Nevada. Absolute value averages are computed to eliminate sign dependency in bias comparisons across datasets.

Model	VR-CESM 0.125°	VR-CESM 0.25° (rough)	VR-CESM 0.25° (smooth)	WRF-9	WRF-27	CESM-FV 0.25°	CESM-SE 1°
DJF Climate Bias (units - mm)							
NLDAS VIC	2.10	2.10	-6.80	-3.70	1.90	16.0	-22.9
NLDAS NOAH	7.20	6.80	-2.10	1.40	6.60	20.7	-16.8
NLDAS MOSAIC	22.3	22.1	13.2	16.5	21.9	36.0	-3.70
MODIS-5	-7.10	-6.10	-15.0	-12.9	-6.30	7.80	-28.5
Reanalysis Dataset Absolute Value Average	9.70	9.30	9.30	8.60	9.20	20.1	18.0
DJF Pearson Pattern Correlation							
NLDAS VIC	0.76	0.79	0.77	0.92	0.84	0.56	0.24
NLDAS NOAH	0.78	0.80	0.77	0.92	0.85	0.60	0.17
NLDAS MOSAIC	0.65	0.69	0.68	0.78	0.76	0.44	0.04
Reanalysis Dataset Average	0.73	0.76	0.74	0.87	0.82	0.53	0.15

LIST OF FIGURES

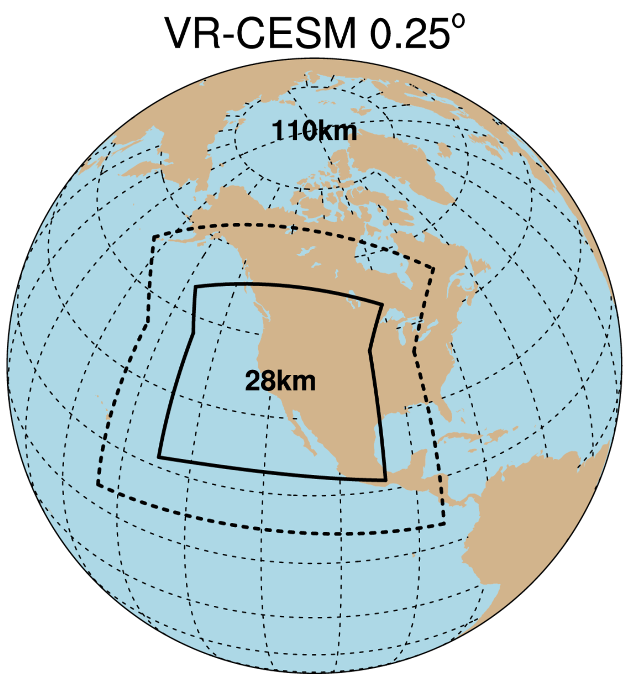

FIG. 1. The two variable-resolution global climate model grids (0.25° (28km), left and 0.125° (14km), right) used for this study. Both grids are developed on a cubed-sphere with a 1.00° quasi-uniform resolution (111km). The dashed lines highlight the model transition region and the solid lines indicate the higher resolution regions.

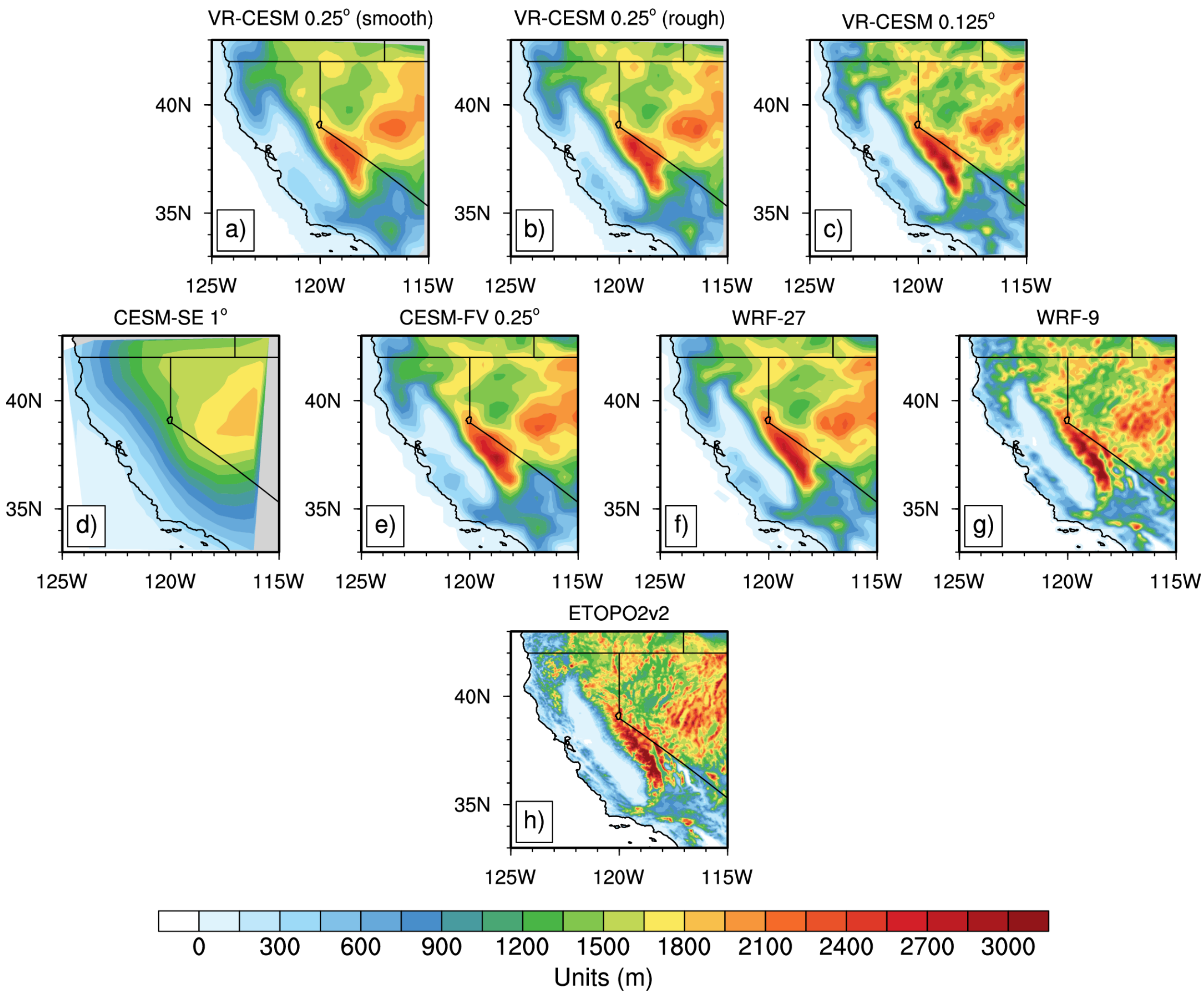

FIG. 2. Topographical representation of the Sierra Nevada mountain range and surrounding regions across model datasets. Topography from variable-resolution CESM is displayed in order of increasing grid resolution from (a) to (c). The standard CESM and WRF simulations are displayed in order of increasing resolution from (d) to (g). The ETOPO2V2 dataset, representing 2-minute (2 km) gridded topographic relief is depicted in (h).

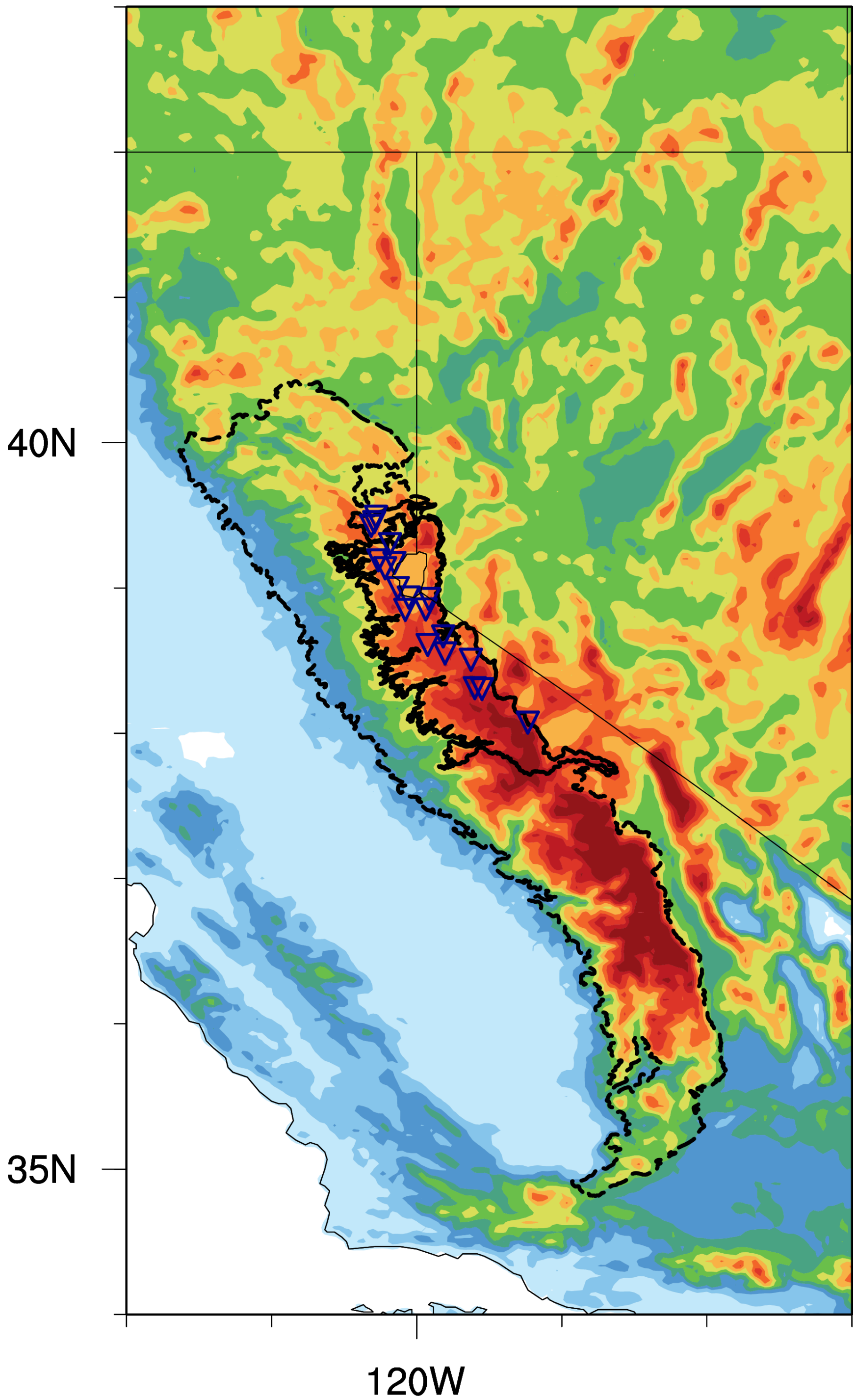

FIG. 3. The EPA's Ecoregion Level III (6.2.12) shapefile mask used for summary statistic calculations of the Sierra Nevada mountain range (dashed black outline). SNOTEL station locations (blue triangles) are overlaid onto the ETOPO2v2 topography. The solid black outline is used to indicate the subregion used to compare model and reanalysis data to SNOTEL stations.

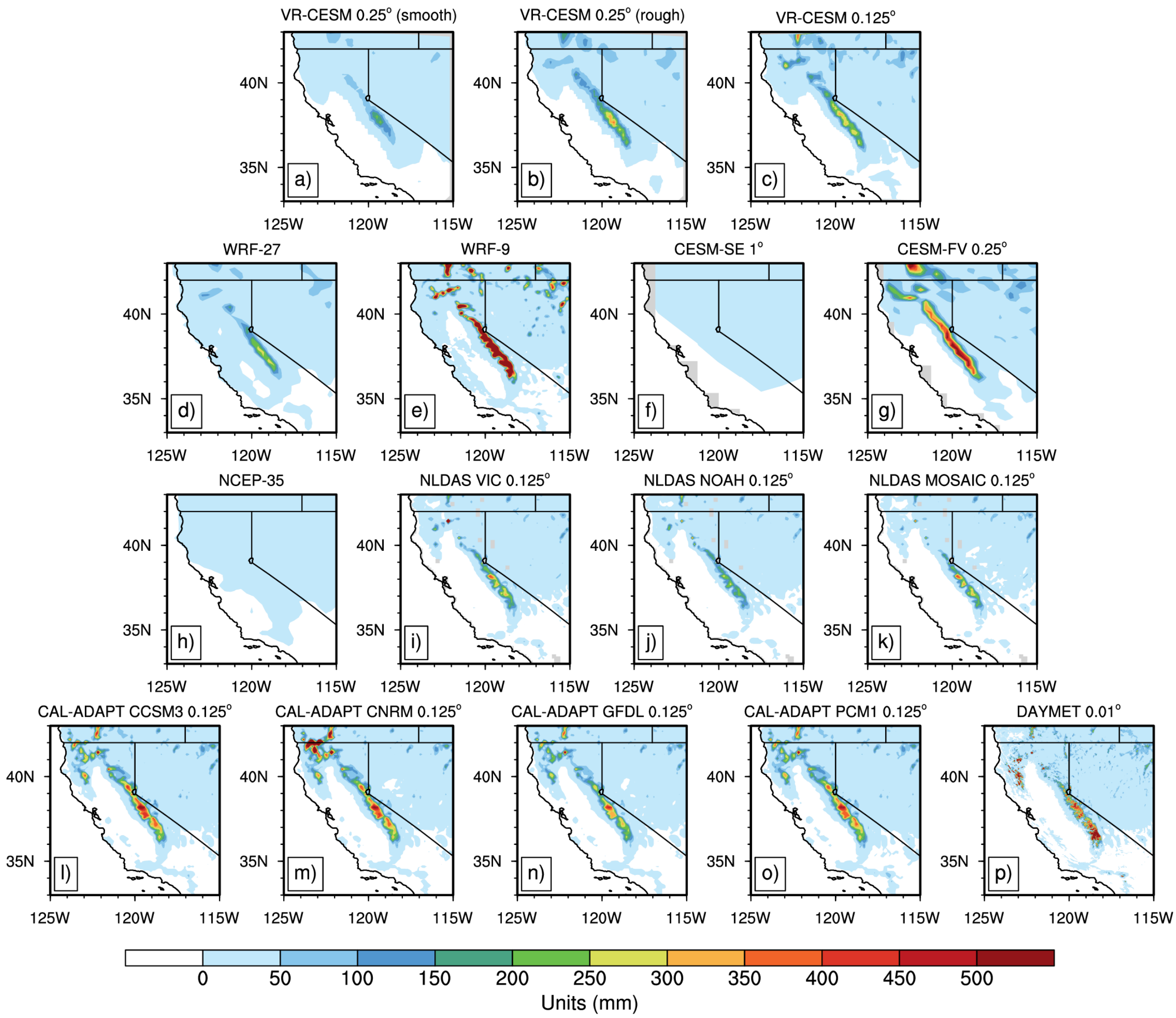

918 FIG. 4. Average climatological DJF snow water equivalent (SWE) across model and observational datasets
919 over California.

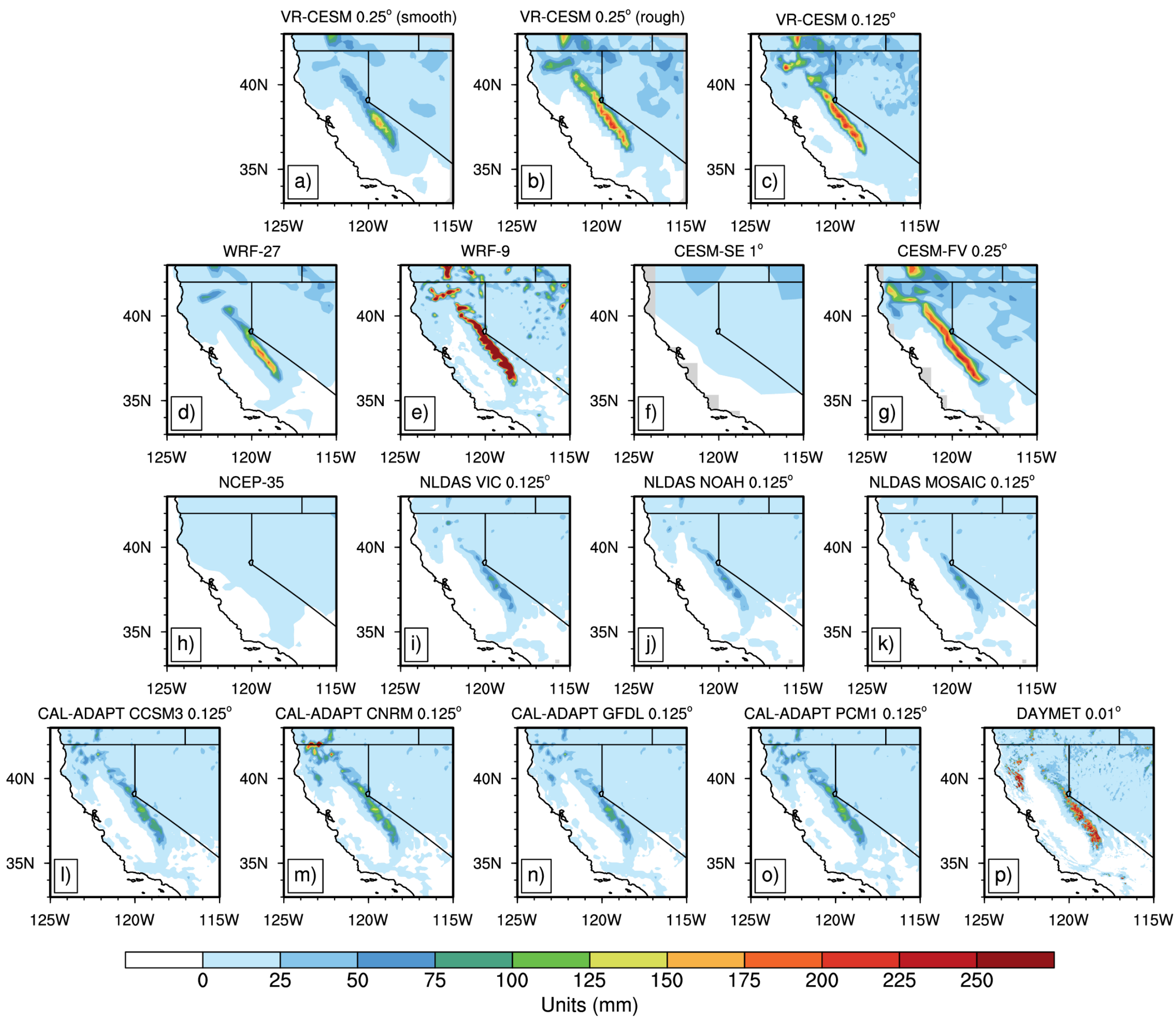

920 FIG. 5. Average DJF variability (interannual standard deviation of the seasonal mean) of snow water equivalent (SWE) across model and observational datasets over California.

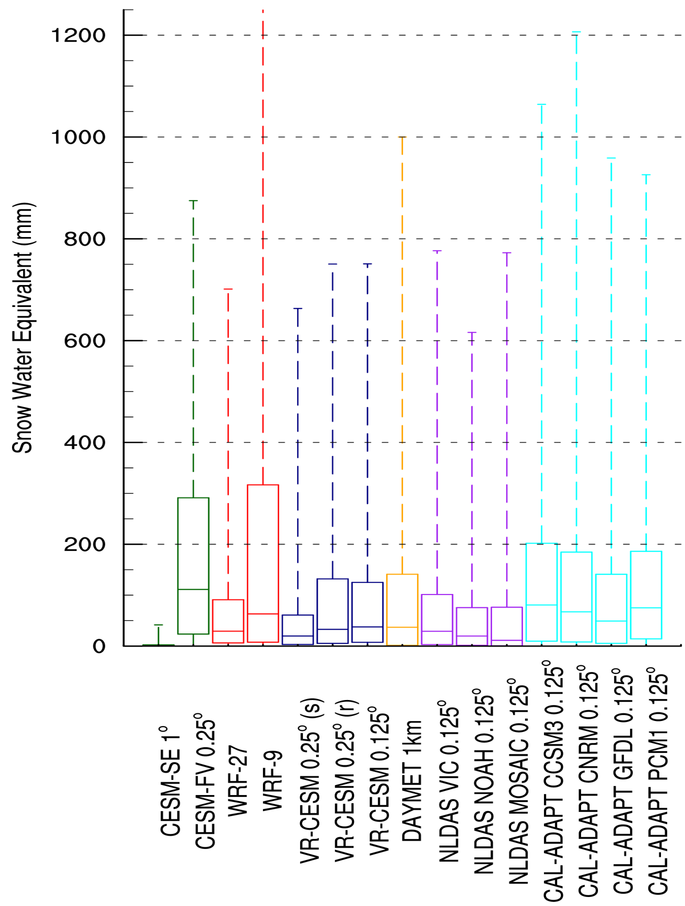

FIG. 6. Boxplots of seasonal (DJF) Sierra Nevada snow water equivalent (SWE) across modeling platforms and observational datasets. The boxes represent the 25th and 75th percentile values within the Sierra Nevada masked region, with the median value indicated in between. The minimum and maximum range is depicted by vertically dashed lines. Regridding of reanalysis datasets to 0.25° (or 0.125° for DAYMET) had no noticeable effect on the statistics and so are not shown.

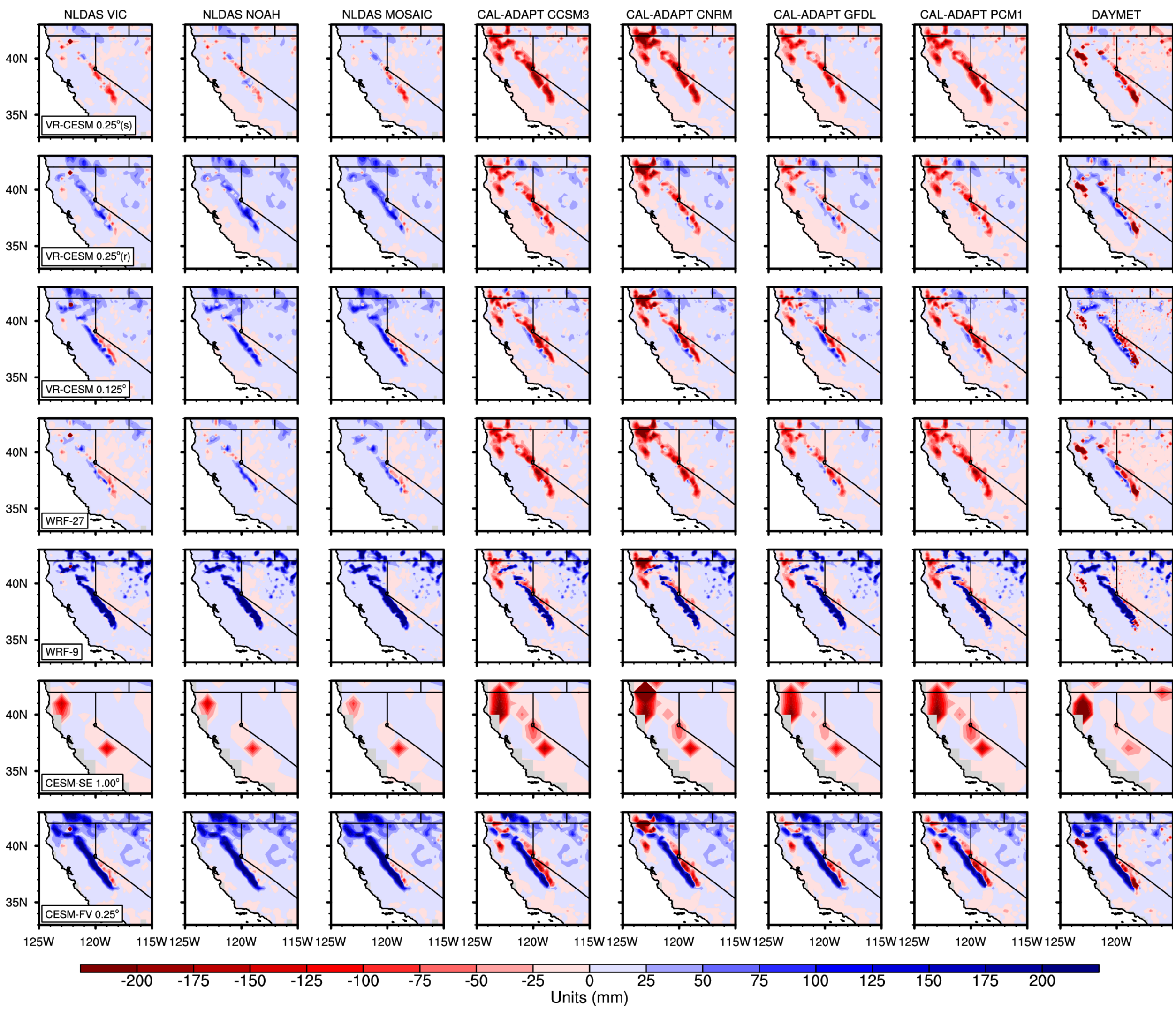

FIG. 7. Average difference in DJF SWE between model and reanalysis datasets over California. Rows indicate model output and columns represent gridded or reanalysis datasets. Blue (red) indicates a model positive (negative) difference in SWE compared to the given reanalysis dataset.

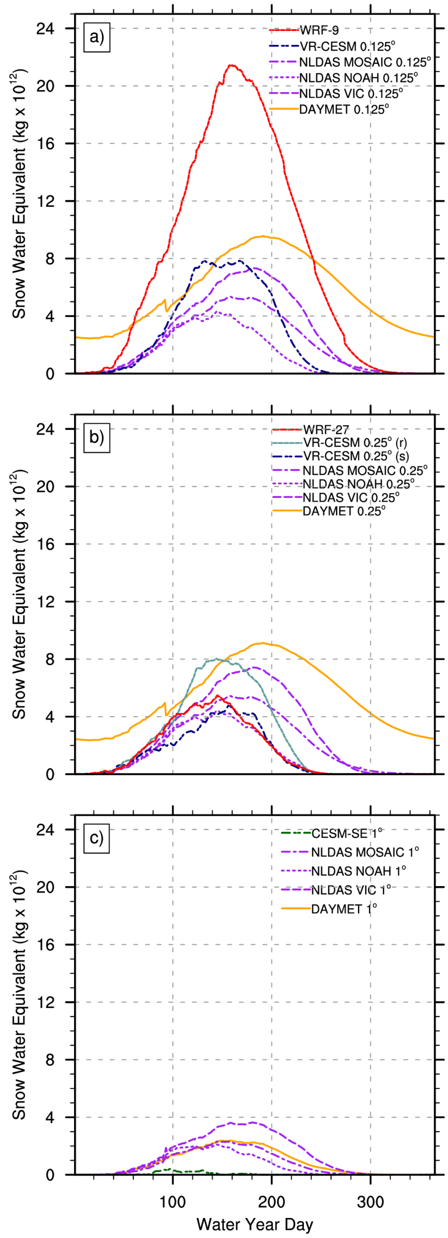

FIG. 8. Average water year day totals for SWE within the Sierra Nevada SNOTEL subregion. Plots are sorted according to the resolution of the models - namely, (a) 0.125° (14km), (b) 0.25° (28km), and (c) 1° (111km). The Sierra Nevada SNOTEL station datast (19 locations) is plotted in black within each diagram. The horizontal axis represents Water Year Day (beginning October 1st through September 31st).

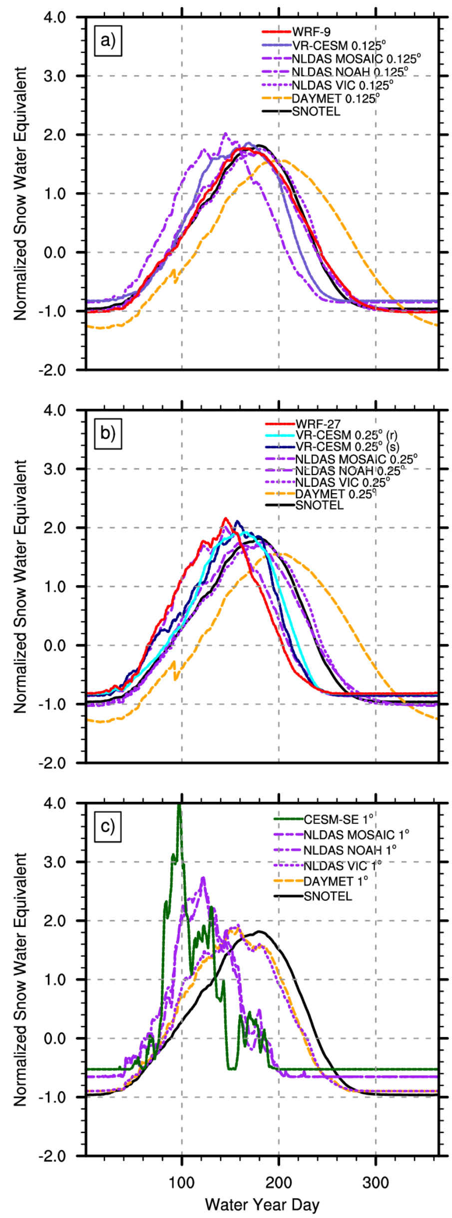

FIG. 9. Normalized average SWE within the Sierra Nevada SNOTEL subregion. Plots are sorted according to the resolution of the models - namely, (a) 0.125° (14km), (b) 0.25° (28km), and (c) 1° (111km). The Sierra Nevada SNOTEL station dataset (19 locations) is plotted in black within each diagram. The horizontal axis represents Water Year Day (beginning October 1st through September 31st).

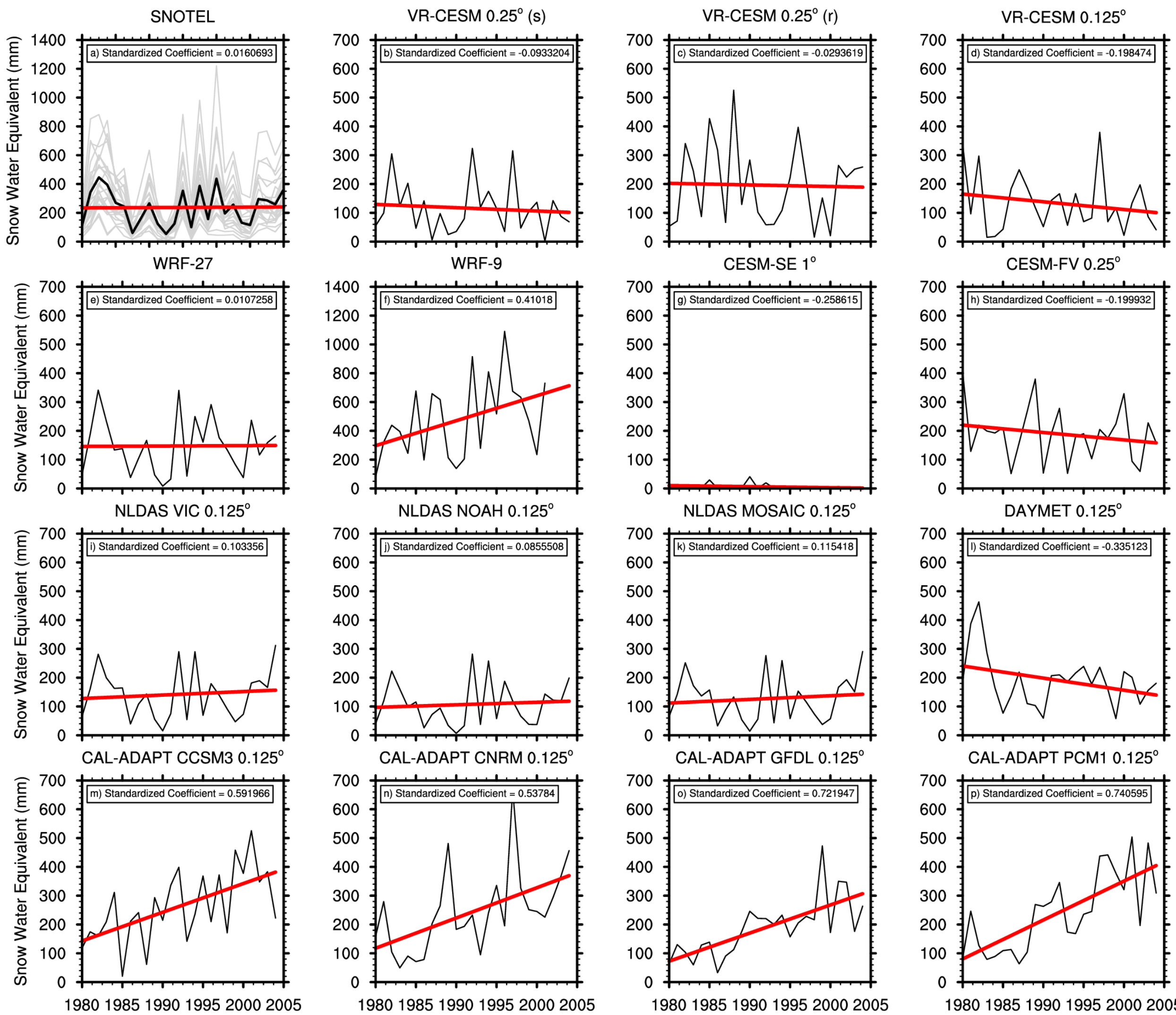

FIG. 10. Linear trend in average seasonal DJF SWE within the Sierra Nevada SNOTEL comparison subregion across model, observational, and reanalysis datasets over the historical period (DJF season 1980 to 2005). The SNOTEL dataset, plot (a), incorporates 19 SNOTEL stations spread throughout the Sierra Nevada that contained 25 DJF seasons of observations. Gray lines indicate individual SNOTEL station with the average seasonal DJF SWE value represented by the black line. Standardized regression coefficient is shown in the upper left corner of each plot.

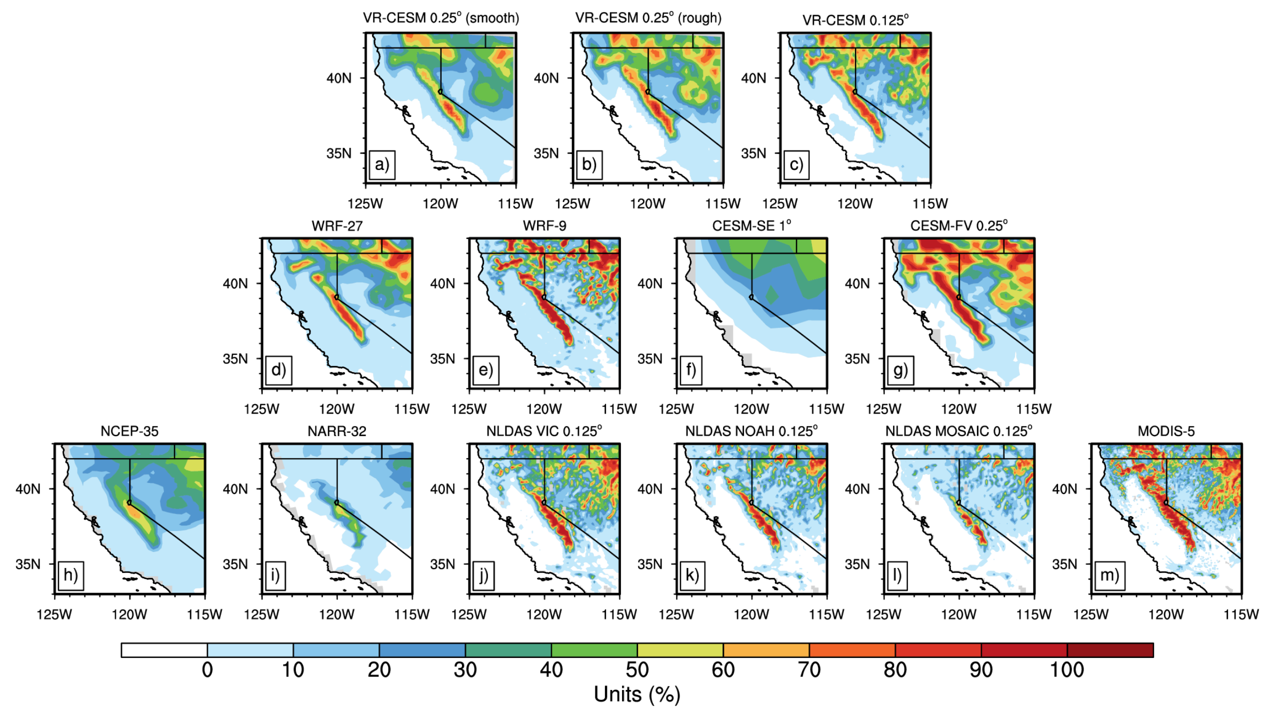

FIG. 11. Average climatological DJF snow cover (SNOWC) across model, observational, and reanalysis datasets over California. The MODIS dataset spans the years 2000-2012.

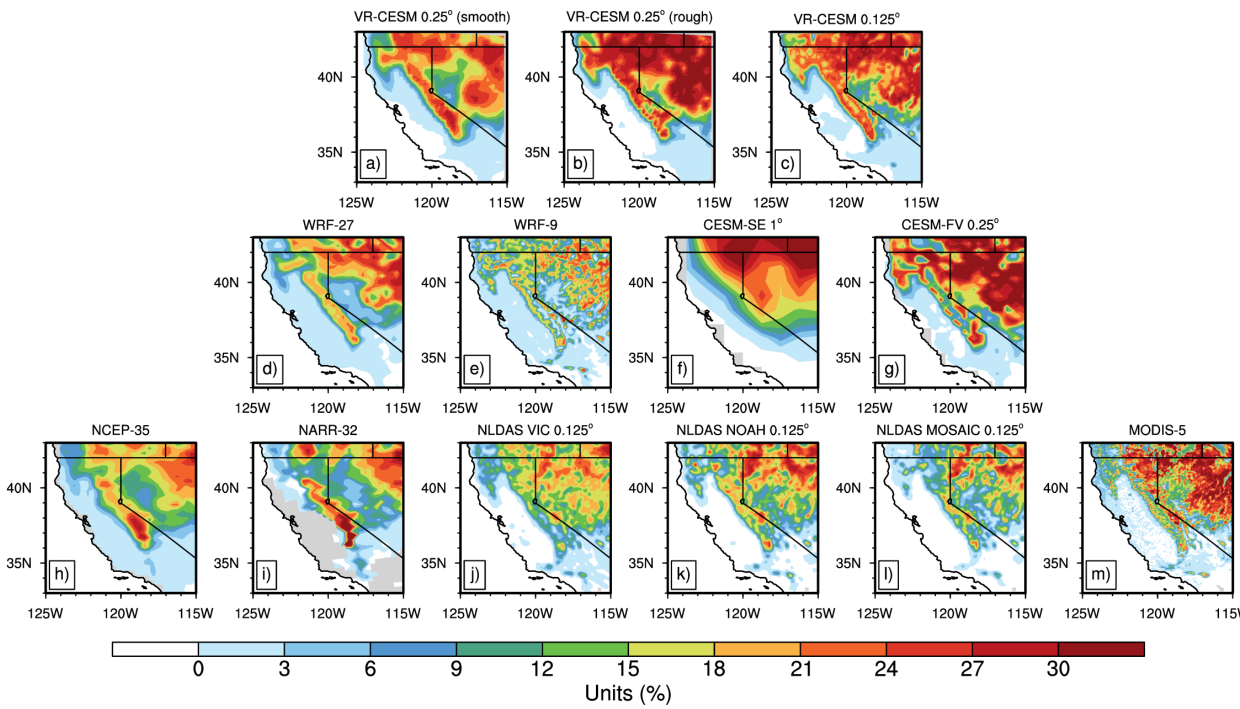

FIG. 12. Average DJF variability (interannual standard deviation of the seasonal mean) of snow cover (SNOWC) across model, observational, and reanalysis datasets over California. The MODIS dataset spans the years 2000-2012.

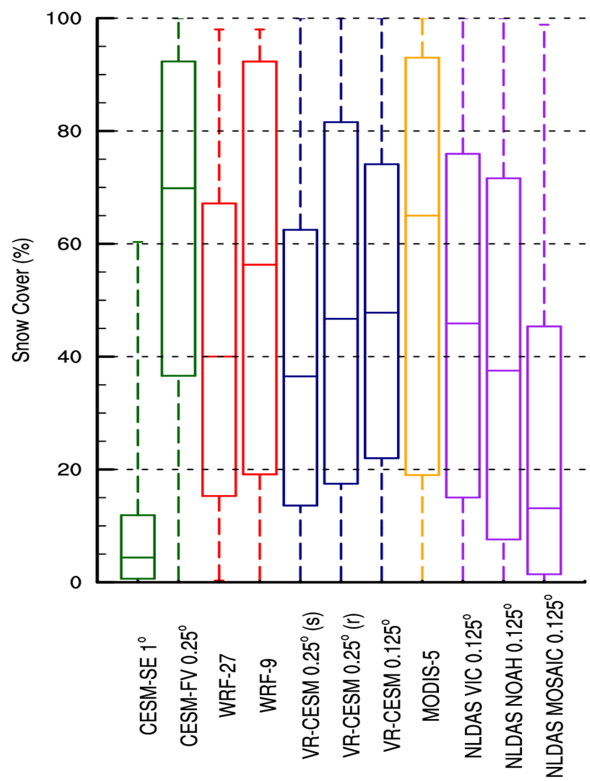

FIG. 13. Boxplots of seasonal (DJF) Sierra Nevada snow cover (SNOWC) across modeling platforms and observational datasets. The boxes represent the 25th and 75th percentile values within the Sierra Nevada masked region, with the median value indicated in between. The minimum and maximum range is depicted by vertically dashed lines. Regridding of reanalysis datasets to 0.25° (or 0.125° for MODIS) had no noticeable effect on the statistics and so are not shown. The MODIS dataset spans the years 2000-2012.

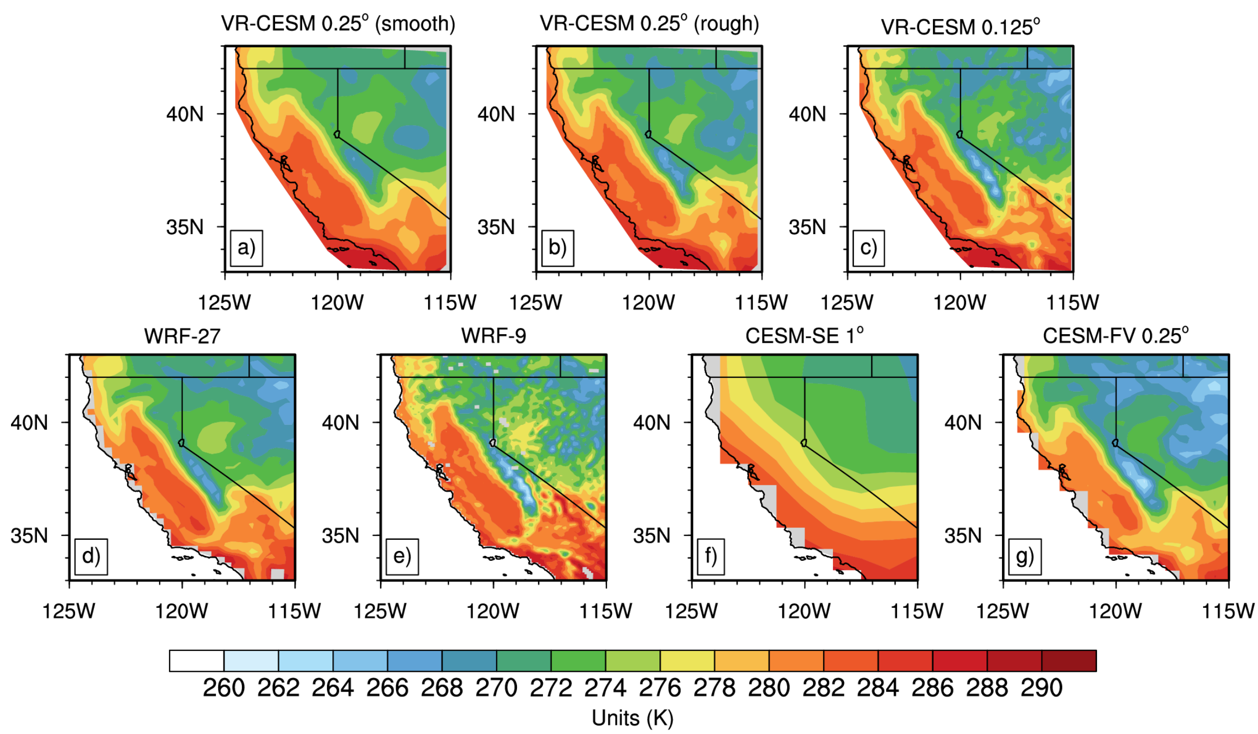

FIG. 14. Average climatological DJF 2m surface temperature across model datasets over California.